

# Phase Curves of Nine Trojan Asteroids over a Wide Range of Phase Angles

Martha W. Schaefer

*Geology and Geophysics and Physics and Astronomy  
Louisiana State University, Baton Rouge, LA 70803, USA  
mws@lsu.edu*

Bradley E. Schaefer

*Physics and Astronomy  
Louisiana State University, Baton Rouge, LA, USA*

David L. Rabinowitz

*Center for Astronomy and Astrophysics  
Yale University, New Haven, CT, USA*

Suzanne W. Tourtellotte

*Department of Astronomy  
Yale University, New Haven, CT, USA*

## Abstract

We have observed well-sampled phase curves for nine Trojan asteroids in B-, V-, and I-bands. These were constructed from 778 magnitudes taken with the 1.3-m telescope on Cerro Tololo as operated by a service observer for the SMARTS consortium. Over our typical phase range of  $0.2\text{-}10^\circ$ , we find our phase curves to be adequately described by a linear model, for slopes of  $0.04\text{-}0.09 \text{ mag}/^\circ$  with average uncertainty less than  $0.02 \text{ mag}/^\circ$ . (The one exception, 51378 (2001 AT33), has a formally negative slope of  $-0.02\pm 0.01 \text{ mag}/^\circ$ .) These slopes are too steep for the opposition surge mechanism to be shadow hiding (SH), so we conclude that the dominant surge mechanism must be coherent backscattering (CB). In a detailed comparison of surface properties (including surge slope, B-R color, and albedo), we find that the Trojans have surface properties similar to the P and C class asteroids prominent in the outer main belt, yet they have significantly different surge properties (at a confidence level of 99.90%). This provides an imperfect argument against the traditional idea that the Trojans were formed around Jupiter's orbit. We also find no overlap in Trojan properties with either the main belt asteroids or with the small icy bodies in the outer Solar System. Importantly, we find that the Trojans are indistinguishable from other small bodies in the outer Solar System that have lost their surface ices (such as the gray Centaurs, gray Scattered Disk Objects, and dead comets). Thus, we find strong support for the idea that the Trojans originally formed as icy bodies in the outer Solar System, were captured into their current orbits during the migration of the gas giant planets, and subsequently lost all their surface ices.

## Introduction

The Trojan asteroids share the orbit of Jupiter, orbiting the sun in two populations at the Lagrangian points of Jupiter's orbit,  $\sim 60^\circ$  leading (L4) and  $\sim 60^\circ$  trailing (L5) that body. The traditional idea was that these asteroids were captured rocky material from near the same orbit as Jupiter (Barucci et al., 2002). Alternatively, Morbidelli et al. (2005) suggested, based on dynamical reasons, that the Trojan asteroids were formed much farther out in the Solar System and were captured into co-orbital motion with Jupiter during the time when the giant planets themselves were migrating, just after Jupiter and Saturn crossed their mutual 1:2 resonance. If these bodies were formed at their present distance from the Sun, then their surfaces would always have been rocky. However, if they were formed much farther out in the Solar System and migrated inward, their surfaces would have originally been icy and would have de-iced since the migration. So we have a question: are Trojans captured asteroids or icy bodies captured during a migration of Jupiter?

If the Trojan asteroids were captured into their present orbits after their formation, then evidence of this should exist in their surface properties. Spectroscopy offers one method to study the dynamical evolution of these bodies. Recent work, for example by Bendjoya et al. (2004), Fornasier et al. (2004), and Roig et al. (2008) indicates that the Trojan asteroids are dominantly of the D taxonomic class, with a small fraction of the members of the P and C classes. Of the Trojans asteroids classified in the JPL Small-Body Database engine, 81% are of class D, 14% of class C, and 14% of class P (there is some overlap). Also from this database, the classified outer main belt asteroids have 20% in the D class, 34% in the C class, and 28% in the P class.

Another way to distinguish the origin of the Trojan asteroids is to compare their phase curves with those of regular asteroids and outer icy bodies. The phase curve of a body is a measurement of the reflected brightness of that body as a function of solar phase angle ( $\alpha$ , here presented in units of degrees), i.e., the angle from the Sun to the object to the Earth. In general, the body's brightness increases as it approaches opposition ( $\alpha \sim 0^\circ$ ) by as much as around half a magnitude. This brightening in the phase curve is called the *opposition surge*, and is the result of one or both of two mechanisms. The first mechanism is shadow-hiding, which is caused by the disappearance of shadows on a surface as the Sun gets behind the observer. The characteristic angular size of the opposition surge here is  $6^\circ$  or larger, and the brightening cannot be more than a factor of two in amplitude. The second mechanism, coherent backscattering, is caused by constructive interference of light rays multiply-scattered by the surface. The characteristic angular size of this surge is from a few tenths of a degree to perhaps  $3^\circ$ , and the amplitude is also restricted to be no more than a factor of two. In practice, surge amplitudes range from 0.03—0.5 mag, with coherent backscattering surges producing fairly sharp spikes in the phase curve, and the shadow-hiding surges leading to shallow slopes over observable ranges of phases ( $0$ — $10^\circ$  for Trojans). For general reviews on phase curves in our Solar System see Hapke (1993), Belskaya and Shevchenko (2000), Muinonen et al. (2002), Rabinowitz et al. (2007), and Schaefer et al. (2009a; b)

Phase curves provide one of the few independent means to compare the Trojans to possible parent populations. With this, we can compare Trojan phase curves with those of Centaurs, dead-comet candidates, and normal asteroids. If the traditional view of the formation of the Trojans is correct, then they should have phase curves comparable to those of normal asteroids from the outer main belt. If Trojans were originally icy bodies from the outer Solar System, then their phase curves should be more like those icy bodies that have suffered extensive volatile loss due to proximity to the Sun, such as dead comets and gray Centaurs. Schaefer et al., 2008b predict that the Trojans will have identical phase curves as the gray Centaurs and the dead-comet candidates.

Thus, the phase curves offer a possible means of distinguishing the origin of the Trojan asteroids. For the comparison, all available phase curves for the outer icy bodies have been collected in Schaefer et al. (2008a; 2009b), and phase curves for the asteroids are presented in Belskaya and Shevchenko (2000) and Muinonen et al. (2002). Prior work on phase curves of Trojan asteroids has been sparse. French (1987) reports on a slope for 1187 Anchises, but this is based on only four nights of data below  $2^\circ$ . What is needed are well-sampled phase curves for many Trojans.

To fill this need, and to test origin hypotheses for the Trojans, we have undertaken three campaigns to obtain well-sampled phase curves. Our photometry of 9 Trojans in the B, V, and I bands was all collected with the 1.3-m telescope on Cerro Tololo in the years 2006—2008. Our results are 9 well-sampled phase curves that we compare to asteroids, Centaurs, and dead comets.

## Data

For this project we used the 1.3 m telescope of the Small and Moderate Aperture Research Telescope System (SMARTS) consortium at Cerro Tololo. Observations were made by on-site operators at Cerro Tololo. Images were recorded with the optical channel (a Fairchild  $2K \times 2K$  CCD) of the ANDICAM (A Novel Dual-Imaging Camera), a permanently mounted, dual infrared/optical CCD camera. We binned the CCD in  $2 \times 2$  mode to obtain  $0.37'' \text{ pixel}^{-1}$  and a  $6.3' \times 6.3'$  field of view. Typical seeing is  $1''$ - $2''$ . This telescope is queue-scheduled for shared use by all members of the SMARTS consortium; therefore we were able to obtain  $\sim 15$  minutes of observing time per target for many nights around solar phase minimum out to near maximum phase. We usually observed two targets per night, often with a sequence of three exposures (B-V-I) per target. Telescope users share dome and sky flats, bias frames, and observations in B, V, and I of Landolt stars on all photometric nights. Our reduction procedure is described in detail elsewhere (Rabinowitz et al., 2006).

Given the time restrictions of the SMARTS queue schedule, we were limited to observing roughly four targets in any one campaign. We made a total of three campaigns, corresponding to the opposition of the L4 cluster in 2006, the L4 cluster in 2007, and the L5 cluster in 2008. Eurysaces, in the L4 cluster, was observed during two campaigns. We selected our targets as being those which have maximum apparent

magnitudes brighter than about 18 and which passed through phases of less than  $0.2^\circ$  (although observing conditions prevented us from obtaining data at below  $0.2^\circ$  in a few cases). In all, we obtained good phase curves for 9 Trojan asteroids: 588 Achilles, 1208 Troilus, 4348 Poulydamas, 6998 Tithonus, 8317 Eurysaces, 12126 (1999 RM11), 13323 (1998 SQ), 24506 (2001 BS15), and 51378 (2001 AT33).

The basic properties of our 9 targets are summarized in Table 1. The number and name (or designation) of each asteroid is given, followed by which group it belongs to (the L4 group, generally named after the Greeks, or the L5 group, generally named after the Trojans). The absolute magnitude (H) and orbital inclination (i) follow, as taken from the NASA Horizons web interface (<http://ssd.jpl.nasa.gov/horizons.cgi>). The last three columns contain the range of dates over which observations were made, the solar phase range of the observations, and the total number of observations (including all three bands as separate observations).

All of our observed magnitudes are presented in Table 2. Due to the length of this tabulation, the table is only presented in electronic form, while a stub of this table (the first 10 lines) is presented in the paper copy, so that readers can see the format and contents of the table.

The first three columns are light-time corrected observation times (in JD minus 2450000) of the observations in the B, V, and I bands. The raw magnitudes and their errors in the three bands are the next six columns. The reduced magnitudes (the apparent magnitudes with the modulation due to the changing distance to the Earth and Sun removed) are listed in the next three columns. Thus, the reduced magnitude is  $B_{red} = B - 5 \log_{10}(r\Delta)$ , where  $r$  and  $\Delta$  are the distances of the target to the Sun and Earth, respectively (in AU). The phase angle (Sun-asteroid-Earth) is in the final column.

The quoted uncertainties in Table 2 are for the measurement errors alone, and these are largely a product of the photon statistics in our images. However, there are additional systematic errors that have to be accounted for to get realistic error estimates. Part of this is an irreducible measurement error of 0.015 mag caused by variations in the CCD chip and recognizable by the scatter in the calibration of standard stars (Landolt, 1992; 2009). Therefore, in our analysis below, we always use the quoted statistical errors added in quadrature with the 0.015 mag systematic uncertainty. We are always using the same telescope and the same filters and the same CCD chip, so this provides us with a remarkable stability over both the short term and the long term. Standard stars (Landolt, 1992) are observed within a few hours (sometimes within a few minutes) of our Trojan fields, and these measures (using large photometric apertures to get nearly all the stars' flux and make the measures insensitive to changes in seeing, focus, or imperfections in centering) are used to calibrate the on-chip comparison stars for use in differential photometry (using small photometric apertures) with respect to the Trojan. We use multiple comparison stars that are substantially brighter than the Trojan, so the added statistical uncertainty from this process is always much smaller than the quoted error bars. The largest uncertainty in this process results from the correction for airmass in deriving the magnitudes of the comparison stars. The Trojan fields are almost always

within a third of an airmass of the Landolt fields. The one-sigma scatter in the fluctuations of the extinction coefficients is 0.04, 0.03, and 0.02 mag per airmass superposed on seasonal variations of total amplitude of 0.03, 0.03, and 0.03 mag per airmass in the B-band, V-band, and I-band respectively (Gutierrez-Moreno et al., 1986; Landolt, personal communication; Rufener, 1986). With this, we expect typical errors in the calibration of the comparison stars caused by uncertainties in the extinction to be around 0.01 mag. But we must always be aware that extinction can change rapidly and some nights can have anomalously high extinction, and this can lead to an occasional magnitude with a substantially larger systematic error. Such errors are essentially impossible to know in practice, so we cannot add them in systematically, nor can we list them individually for each magnitude. While expected to generally be relatively small, this extinction calibration systematic error will be subsumed into the likely larger uncertainty associated with the rotation of the Trojan.

Therefore, we have added an arbitrary value for the systematic error ( $\sigma_{\text{sys}}$ ) in quadrature with our measurement error to produce an estimate of the total error bar. The value of the systematic error for each asteroid has been chosen such that our model fits (see next section) produce a reduced  $\chi^2$  of near unity. As such, the fact that our model fits have reduced  $\chi^2$  near unity is by construction. Our derived  $\sigma_{\text{sys}}$  values for each of the nine targets are presented in the third column of Table 3. For some of our asteroids (for example, 588 Achilles), the  $\sigma_{\text{sys}}$  value is sufficiently small that any rotational modulation effects must be negligible. However, one of our asteroids (51378 (2001 AT33)) has an unexpectedly large  $\sigma_{\text{sys}}$ , which indicates substantial rotational modulation, for which we have not been able to determine a period. Nonetheless, we show below ("Rotational Modulation") that any rotational modulation is unlikely to significantly alter the slope we derive for the phase curve.

The reduced magnitudes ( $B_{\text{red}}$ ,  $V_{\text{red}}$ , and  $I_{\text{red}}$ ) in B, V, and I taken sequentially during a single night were averaged together to produce a single magnitude  $m_{\text{avg}}$ . The combination of the three filters is justified by the lack of any significant difference between the slopes. This color neutrality of the surges has a good precedent that all other known surges from small/gray objects are closely neutral (Schaefer et al., 2009b). Also, the excellent phase curve for Achilles shows a difference in slope of only 0.002 mag/ $^\circ$  from V-band to R-band (Shevchenko et al., 2009). The JD of these observations were similarly averaged. If BVI sequences were taken more than once during a night, two magnitudes ( $m_{\text{avg}}$ ) are reported. In cases where only a partial sequence was observed, the color of the object is assumed constant with time, and the mean B-V, V-I, or B-I (depending on which values were available) was used to calculate the missing value, which was then averaged as before. This procedure was performed in about a third of the BVI triplet sequences (almost all 8317 Eurysaces and 13323 (1998 SQ)).

## Analysis

Phase curves are plots of the reduced magnitudes versus the phase angle. The error bars on our individual magnitudes are taken to be the total uncertainties, i.e.,

including the systematic error bars as described above. Our derived phase curves are plotted for all nine objects in Figures 1—9.

Our phase curves are well-sampled in phase and cover essentially all the observable range of phase angles. These phase curves show the usual opposition surge with a brightening towards low phase angle. The only exception is for 51378 (2001 AT33), which apparently is dimming as zero phase is approached.

Many asteroids display rotational modulation with significant amplitudes. These variations are uncorrelated with the phase angle and hence, if uncorrected, will introduce perhaps substantial scatter in any phase curve. We expect that uncorrected rotation effects will indeed be the dominant source of scatter in our phase curves. Of these nine Trojans, only 588 Achilles (Shevchenko et al., 2009) and 1208 Troilus (Molnar et al., 2008) now have known rotational periods, and we have not been able to determine any further confident rotational modulation in our data. We have performed Fourier transform analyses of all our light curves and all targets always have some highest peak in the Fourier transform. These highest peaks might be the real rotational period (or an alias of the real period), but we cannot prove that this is the case for any of the targets. Nevertheless, we have decided to remove the putative rotational modulation for the highest Fourier peak for all targets. However, this removal does not have a significant influence on the calculated phase slopes. Figures 1—9 show the phase slopes before the removal of the putative rotational modulation.

We fitted all of the phase curves to two models: a simple empirical linear fit, and a fit to the Hapke model (Hapke, 2002) for opposition surges. For empirical models, we chose the linear fit because it is the simplest possible model for the surge and this provides a fully adequate representation of the data. We also chose to fit the Hapke equations because this is a physics-based model. A difficulty with this model is that the resultant fit parameters are somewhat degenerate, for example between the contribution from shadow hiding (SH) and coherent backscattering (CB). We have chosen to not fit the H-G formalism because there is no physics in it, while as a purely empirical functional form, there is no reason to go to this complexity when a simple line fits well.

The linear fits to the phase curves were made by minimizing the  $\chi^2$  comparison between the model and the data. The model equation is  $m_{\text{avg}} = m_0 + S\alpha$ , where  $\alpha$  is the phase angle (in  $^\circ$ ),  $S$  is the slope of the phase curve (in  $\text{mag}/^\circ$ ),  $m_0$  is the absolute magnitude of the body at zero phase angle, and  $m_{\text{avg}}$  is our average reduced magnitude. The best fit values for all the data are presented in Table 3. We have also performed fits for just the data that have  $\alpha \leq 2^\circ$  and for  $\alpha > 5^\circ$ , with the resulting slopes  $S_{\leq 2}$  and  $S_{> 5}$  being tabulated in Table 3.

The columns in Table 3 are as follows: name of asteroid; number of observations ( $N_{\text{obs}}$ , considered to be the number of  $m_{\text{avg}}$  for each asteroid);  $\sigma_{\text{sys}}$  (described above); and the linear fit parameters: average phase slope ( $S$ ) in  $\text{mag}/^\circ$ , absolute magnitude at zero phase angle ( $m_0$ ) in  $\text{mag}$ , the  $\chi^2$  of the linear fit, and the other slopes  $S_{\leq 2}$  and  $S_{> 5}$  in  $\text{mag}/^\circ$ ; the parameters of the Hapke fit are described below. The  $\chi^2$  values for the linear and

Hapke fits are such that the smaller of the two reduced  $\chi^2$  values is unity by construction, as described above.

The average slope,  $S$ , is  $0.06 \text{ mag/}^\circ$ , with a range of  $0.04\text{--}0.09 \text{ mag/}^\circ$ , and with a surprisingly low RMS scatter of  $0.02 \text{ mag/}^\circ$ . (For the statistics in this paragraph, we will ignore 51378 (2001 AT33), which has an anomalously negative slope.) The average slope at phase less than or equal to  $2^\circ$  is not significantly different than at phase greater than  $5^\circ$  (both  $0.05 \text{ mag/}^\circ$ ). This implies that our slopes do not greatly deviate from linearity. (Indeed, this will be seen later as the best-fit Hapke models do not have significantly better  $\chi^2$  values than do the best-fit linear models.) While the linear models are good approximations to the observations, they do not reflect the known physics of the surge mechanisms.

Phase curve data were also fit to a Hapke model (Hapke, 2002) as follows. For our case of small phase angles, the observed magnitude is

$$m = m_* - 2.5 \times \log_{10}[p(1 + B_{S0}B_S) + M] - 2.5 \times \log_{10}[1 + B_{C0}B_C], \text{ where}$$

$$B_S = (1 + [\tan(\alpha/2)]/h_S)^{-1},$$

$$B_C = 0.5(1 + [(1 - e^{-Z})/Z])/(1 + Z)^2,$$

$$Z = [\tan(\alpha/2)]/h_C.$$

Here,  $m_*$  is a magnitude that has absorbed various constants,  $p$  is the single particle scattering function evaluated for  $\alpha \sim 0^\circ$ , and  $M$  is the multiple scattering contribution. The contribution to the opposition surge from shadow hiding is given by  $B_S$  with an amplitude of  $B_{S0}$  and a width of  $h_S$ . The contribution to the surge from coherent backscatter is given by  $B_C$  with an amplitude of  $B_{C0}$  and a width of  $h_C$ . There are limits on the amplitudes from the physics of both mechanisms, such that  $B_{S0} \leq 1$  and also  $B_{C0} \leq 1$ .

Through  $\chi^2$  minimization, we tested several models for the opposition surge of these bodies: shadow-hiding only, coherent backscattering only, and coherent backscattering with maximal shadow-hiding. For example, for our best-observed target (8317 Eurysaces) we fitted a variety of surge models. For shadow-hiding alone, our best fit with a restriction that  $h_S \geq 6^\circ$  results in a  $\chi^2 = 346$ . This  $\chi^2$  can be substantially improved (to  $\chi^2 = 245$ ) by lowering  $h_S$  to  $1.2^\circ$ , but this is unphysical, so we do not accept this fit. For coherent backscattering alone, we find a much better fit (with  $\chi^2 = 106$ ) for  $h_C = 4.6^\circ$  and the  $B_{C0}$  value pegged at 1.0. When  $B_{C0}$  is lowered below this value, the  $\chi^2$  is always increased. The comparison of these results (SH alone vs CB alone) for 8317 Eurysaces and the others observed here demonstrates that shadow-hiding does not dominate the opposition surge of the Trojans.

When shadow-hiding is added to the coherent backscattering the best fits are little influenced by varying the SH parameters. For Eurysaces, our best fit SH+CB model produces a  $\chi^2 = 98$ , for  $h_C = 7.3^\circ$ ,  $B_{C0}$  pegged at 1.0, and  $h_S$  pegged at  $6^\circ$ , and  $B_{S0}$  pegged at 1.0. The reason for this is that the SH contribution is relatively flat, and at best can contribute only a small tilt to the modeled phase curve. Because our observed phase curves are largely linear, with small curvature, we cannot evaluate the SH contribution because the model fit parameters become degenerate. However, the overall contribution

from SH must be small compared to the CB contribution, and can be neglected. For simplicity, we will only be reporting on the best fit model for CB alone. Our quoted error bars will only account for the uncertainties within the CB-only model, and these uncertainties would rise somewhat if we allowed a range of models including SH.

Our fits to the data with the Hapke model are summarized in Table 3. The final four columns in Table 3 present the best-fit Hapke parameters for the absolute magnitude at zero phase angle ( $m_0$ ) in mag, coherent backscattering width ( $h_C$ ) in degrees, coherent backscattering amplitude ( $B_{C0}$ ), and the  $\chi^2$  of the fit. We find that in all cases the amplitude of the coherent backscattering is always pegged at its maximum value ( $B_{C0} = 1$ ). The average width for coherent backscattering is  $h_C = 7.5^\circ$ , with a range from  $4.5^\circ$  to  $10.3^\circ$ . The object 51378 (2001 AT33) has a negative slope and no realistic Hapke fit.

We do not understand why the phase curve of 51378 (2001 AT33) has a slightly negative slope. It might be that there are additional phenomena that counteract the opposition surge, but we do not know of any such mechanism. We have no reason to believe that there are systematic errors, because the negative slope would require correlated errors in magnitudes determined independently on many nights. It is not impossible that rotational modulation could have this effect, but we have found no evidence for such. We know of no precedent for a negative phase slope among any asteroids or icy bodies. Perhaps the answer is just that the real phase curve is nearly flat, and ordinary random measurement errors make it appear to have a slightly negative slope. There is precedence for such a flat phase curve for one other small gray body -- the centaur 2002 GZ232 (Schaefer et al., 2009b). Based on this, we can expect about 1 in 10 of the small grey centaurs to have completely flat phase curves, which is consistent with what we are seeing for the Trojans.

## Rotational Modulation

All asteroids rotate, typically with periods from a few hours to a few days, so in principle they should all show some rotational modulation superposed on top of the phase curve. This modulation will be near zero for round and uniform bodies, while typical modulation amplitudes (peak to peak) are 0.1 mag or smaller, yet with some amplitudes getting up to a quarter or a third of a magnitude. Without correction, these rotational modulations will cause deviations from a smooth phase curve. Of the nine Trojan asteroids we observed, only 588 Achilles (Shevchenko et al., 2009) and 1208 Troilus (Molnar et al., 2008) now have known rotational periods, so we have to be concerned with the effects of uncorrected rotational modulation on our derived phase curves and slopes.

In general, uncorrected rotational modulation will not result in any significant changes in our results. The reasons are two fold: (1) we sample our phase curves with numerous observations spread widely in time and solar phase angle; and (2) rotational modulation is (almost) never correlated with the orbital phase. With this, the scatter in our plots will be somewhat larger, while the derived slopes and Hapke parameters will be

nearly the same (although with somewhat larger error bars). We performed a quantitative analysis of this. In particular, we have measured the effects on the derived phase curve slope as the rotational period is varied from 0.1 to 10 days. We have adopted a sinusoidal modulation for this analysis. The analysis has been performed for the exact times and phases as observed for each of the Trojans. For our best-sampled Trojan (Eurysaces), for a peak-to-peak amplitude of 0.10 mag, the RMS scatter of the error in the phase curve slope is 0.0008 mag/°. All of the uncertainties related to rotational modulation will scale linearly with the amplitude, so a rotational modulation with an amplitude of 0.20 mag will have an added uncertainty of 0.0016 mag/°, and so on. For a much more poorly-sampled Trojan (Troilus), again with an amplitude of 0.20 mag (Molnar et al., 2008), the extra error in the slope will be 0.026 mag/°. In general, the extra uncertainty arising from uncorrected rotational modulation will be smaller than our reported uncertainties (see Table 3). The extra RMS scatter in our phase curves will be a factor of  $2^{-1.5}=0.35$  times the amplitude. If all of the scatter in our phase curves above that introduced by the statistical errors in the magnitudes (i.e.,  $\sigma_{\text{sys}}$  as in Table 3) is caused by rotational modulation, then the amplitude should be near  $\sigma_{\text{sys}}/0.35$ . Thus, a number of our Trojans could well have amplitudes of near a quarter of a magnitude, leading to a larger than expected scatter in our phase curves. Nevertheless, for the results of this paper (essentially, the slopes of the phase curves), rotational modulation will not cause any significant changes.

There is one weak exception to this strong conclusion, and that is if the rotational period is close to one day (or half a day), so that the timing of our images (roughly at the same sidereal time each night) might end up being correlated with the phase. Let us illustrate this effect with a specific example where a Trojan has 70 days of observations before opposition all at the same sidereal time each night. If the rotational period is exactly one sidereal day, then our magnitudes would always be at the same part of the rotational modulation, and no change in the slope of the phase curve would result. But if the rotational period is 1/140 days shorter than the sidereal day, then the rotational modulation will change smoothly by exactly half a period over the observed time interval. In this case, if the rotational modulation happened to be near minimum at the start of the 70 day interval and hence near maximum at the end, then the resulting phase curve would have a systematic shift with the high phases being faint and the low phases being bright, resulting in an incorrect slope. In this extreme case, the error in the derived phase curve slope will be the amplitude divided by the range of the covered phase. For a typical amplitude of 0.10 mag and a phase range of 10°, the introduced error in the slope will be 0.01 mag/°. Such extreme cases are very unlikely because they require a fine-tuned period, a fine-tuned epoch of maximum light, and a large amplitude for the rotational modulation. The extreme cases are never reached because our observations have substantial scatter around some idealized identical sidereal time each night. Thus, under rare circumstances, a rotational modulation can produce a systematic change in the slope of the phase curve, but in practice, these effects must be small.

We can be quantitative on these effects for our Trojan phase curves. For the exact times and phases of our Eurysaces data, with a presumed rotational amplitude of 0.10 mag, the error in the slope of the phase curve will always be below 0.009 mag/° for all

periods. As an illustration, for the exact times and phases of our Troilus data, if the rotational amplitude was 0.10 mag, the error in the slope would be less than 0.02 mag/° (our one-sigma uncertainty in the slope from Table 3) for periods outside the range of 0.452-0.454, 0.477-0.481, 0.908-0.926, and 0.962-0.981 days. In fact, Molnar et al. (2008) have found that the rotation period is 2.3405 days, so there is no correlation between orbital phase and rotational phase.

The phase curve for 51378 (2001 AT33) has a formally negative slope, and we had previously wondered whether this could be due to rotational modulation. For the exact times and phases of our data series, and for a rotational amplitude of 0.34 mag ( $\sigma_{\text{sys}}/0.35$ ), we can get slope errors of 0.02 mag/° or larger for periods of 0.496-0.498, 0.501-0.502, 0.974-0.978, 0.984-0.995, 1.002-1.013, and 1.020-1.022 days. Again, there is less than a one percent probability that the true rotational period is in this range. If this possibility is realized, then the severe alias problems would prevent us from discovering the rotational period. The largest possible shift in the slope of the phase curve is 0.04 mag/°, so the rotationally corrected phase curve could have a positive slope up to 0.02 mag/°, which is still substantially flatter than all the other Trojans. Thus, 51378 remains an anomaly even with the unlikely possibility of systematic effects from rotational modulation.

Achilles can provide a test case to determine the importance of the rotational modulation. After our poster was presented at the 2008 DPS meeting in Cornell (Schaefer et al., 2008b), Shevchenko et al. presented an abstract for a well-observed rotational period and phase curve at the 2009 Lunar and Planetary Science Conference. The rotational modulation has a period of 7.306 hours, while showing a double-peaked light curve with the larger of the two peaks having an amplitude of 0.11 mag. For the 2007 opposition, the coverage is from 0.08°-9.72°, with the closely linear phase curves fitted with slopes of 0.045±0.001 and 0.043±0.001 mag/° in the V-band and R-band. This is identical with our result of a linear phase curve with a slope of 0.04±0.01 mag/° for phases 0.165°-8.202°. Shevchenko et al. (2009) used a massive observing campaign involving 13 people and four telescopes so as to get the slope accurate to 0.001 mag/°, whereas this degree of accuracy is not necessary for our calculations. So we view the excellent phase curve from Shevchenko et al. (2009) as good confirmation that our observations and methods are returning good phase curves (despite not having rotational corrections). Their results also provide further experience that the Trojans have phase curves that are closely linear and without significant variations with color.

The issue of correction for rotational modulation is an old one. Ideally, our community would like to have all phase curves corrected with a confident rotational light curve (for example, Shevchenko et al. (2009)), but this is generally not possible (for example, in the present work). Indeed, our field has an extensive literature of reported phase curves based on just a few magnitudes from within two or three small ranges of observed phases and no rotational corrections (e.g., Buratti et al., 1992; Degewij et al., 1980; Sheppard and Jewitt, 2002; Sheppard, 2007), for which any rotational effects are substantially worse than in this paper. The cost in time and money to get a rotational light curve (which requires many closely spaced nights of dedicated telescope time) in

addition to a phase curve (which requires nights well spread throughout an observing season) is generally large. For most science questions (like the cause of the surge and the morphology of surges between classes of bodies), high accuracy ( $\pm 0.001 \text{ mag}/^\circ$  versus  $\pm 0.01 \text{ mag}/^\circ$  or even  $\pm 0.03 \text{ mag}/^\circ$ ) is not needed.

Our analysis has quantitatively demonstrated that our lack of rotational corrections only adds a small additional uncertainty in the slope of our observed phase curves, and these effects do not change any of our conclusions.

## Cause of the Opposition Surge

Two physical mechanisms have been proposed for the opposition surges, shadow hiding and coherent backscattering. To get physical information from observed phase curves, we must determine the cause of the surges. More correctly, as both causes must work at some level, we must determine which mechanism dominates over which phase ranges. Schaefer et al. (2009b) develop four criteria for distinguishing between the mechanisms based on observed properties. The first criterion is that CB must dominate if the surge is color dependent (i.e., the slope varies significantly with color), because shadows are essentially the same for all optical wavelengths. The Trojans have no significant color dependence, and this could arise from either SH or CB. The second criterion is that CB must dominate if the slope is significantly greater than  $0.033 \text{ mag}/^\circ$ , with that being the maximal slope for SH due to its surge width being wider than  $6^\circ$  or so. This criterion is one that we can apply to our Trojan phase curves. The third criterion is that the exact shape of the phase curve will depend on the mechanism, as shown by the different shapes in equations in the Analysis section. Unfortunately, very high accuracy is required to make any useful distinctions, and so our Trojan phase curves cannot be used for this third criterion. The fourth criterion is that CB must dominate if the bodies albedo is larger than  $\sim 40\%$ , with the reason being that high albedos will cause the shadows on the surface to be filled in and hence SH will have only small effect. The Trojans all have very low albedos, so this fourth criterion is not useful as either SH or CB could dominate for low albedo surfaces. In all, we are only left with one useful criterion, the second, for determining the dominant surge mechanism on the Trojans.

From Equation 1, the SH mechanism will have some steepest possible slope. Schaefer et al. (2009b) have derived the slope at zero phase to be  $\approx 0.2(B_{S0}/h_s) \text{ mag}/^\circ$ . The physics constrains  $B_{S0} \leq 1$ . We have an additional constraint that  $h_s \geq 6^\circ$ , either theoretically or empirically. The width of the SH surge will be given by the average size of the shadow caster divided by the length of the shadow cast. For normal geometry of a jumbled surface, the ratio cannot be too small as the porosity of surfaces is not high. Detailed theoretical models of packed particles return similar results (Hapke 1993). Empirically, for the cases where the SH and CB component can be distinguished, the typical value of  $h_s$  ranges from  $10^\circ$ - $40^\circ$  and is never smaller than  $6^\circ$  (e.g., Buratti and Veverka (1985); Helfenstein et al. (1997); Stankevich et al. (1999); Verbiscer et al. (2005)). With these two constraints, the slope at zero phase can only be smaller than  $0.033 \text{ mag}/^\circ$ . We are reporting on the phase curve slopes out to many degrees, and so the

fitted slope over these extended ranges must be smaller than  $0.033 \text{ mag}/^\circ$ . For slopes over phases less than  $2^\circ$ , shadow-hiding must have  $S_{\leq 2}$  less than  $0.026 \text{ mag}/^\circ$ , and for typical values of  $B_{S_0}$  the slope is usually only  $0.01 \text{ mag}/^\circ$ . As such, we have a confident criterion for distinguishing between SH and CB; if the slope is significantly greater than  $0.026 \text{ mag}/^\circ$ , then we can confidently identify CB as the dominant surge mechanism.

Of our nine Trojans, eight have slopes that are steeper than the maximal SH phase curve. Then, by our second criterion, the CB mechanism must be dominating. The one exception is 51378 (2001 AT33), for which the formal slope is slightly negative, for which neither the SH nor the CB models are consistent. In this exception, our second criterion cannot be applied, with some other effect (perhaps rotational modulation) dominating. So eight out of eight Trojans, for which our second criterion can be applied, have the CB mechanism dominating.

## Comparison with Other Groups

To determine the provenance of the Trojan asteroids, we compare them to other groups. The groups with which we can compare our sample are the main belt asteroids, the de-iced outer Solar System bodies, and the icy outer Solar System bodies. The main belt asteroid group objects we compare have surface taxonomy classes including D, P, C, M, S, and E. The de-iced outer Solar System objects (the ‘Small/Gray’ class of bodies) we include are the gray Centaurs, the gray SDOs, and the dead comet candidates. The icy outer Solar System bodies (the ‘Small/Red’ bodies) include Kuiper Belt objects (KBOs) and red Centaurs. No one expects that the Trojans will have surfaces like the icy outer Solar System bodies, but this group is compared here for completeness. We also include comparisons with the transition bodies between the Small/Gray and Small/Red classes, including active Centaurs and active comets.

To make these comparisons, we have collected a variety of properties for each class of bodies into Table 4. These include the surge slopes for phase angles  $\leq 2^\circ$  ( $S_{\leq 2}$ ), the number of bodies for which this was measured ( $N_{\leq 2}$ ), the surge slope  $> 5^\circ$  ( $S_{> 5}$ ), the number of bodies for which this was measured ( $N_{> 5}$ ), the B-R color (corrected to the solar color index), and the albedo.

The Trojans have greatly different properties from the Small/Red bodies, with all measured properties being disjoint in range. Because the Small/Red bodies have icy surfaces, we only have the expected conclusion that the Trojans do not have icy surfaces. The Trojans have similar colors and albedos as the transition bodies, but only to the extent that the transition bodies are like the Small/Gray bodies. We have only one measured surge value for a transition body, and that is outside the range for Trojans but is within the range of the Small/Red bodies. The Trojans also have greatly different surges, colors, and albedos when compared to the M, S, and E asteroid types. We conclude that the Trojans do not share an origin with the main belt asteroids and are not simply ‘captured’ main belt asteroids.

The two competing hypotheses for the origin of the Trojans are that they formed at around the distance of Jupiter (the ‘traditional’ idea) or that they formed much farther out in the Solar System (Morbidelli et al., 2005). The Small/Gray bodies provide a good comparison sample for the far-out origin, and indeed, Schaefer et al. (2008a; 2009b) have made a specific prediction that the Trojans will have an identical distribution of surge properties as the Small/Grays. But we do not have any confident sample of bodies that formed about the orbital position of Jupiter. After all, the Trojans are the question at hand, and everything else has been scattered away. The best that we can do for a comparison sample is the D, P, and C class asteroids that predominate in the outer main belt. It is reasonable that these classes are the most similar to bodies formed around Jupiter’s orbit. That is, perhaps the conditions in the outer main belt make for surfaces similar to those of bodies somewhat farther out. Indeed, most Trojans with spectral classification are placed into the D class (with the remainder being placed in the P and C classes). So, for testing the traditional idea that the Trojans formed around Jupiter’s orbit, the best available group for comparison is the D, P, and C asteroids in the outer main belt, even though it is not quite the correct comparison.

How do the Trojans compare with the Small/Gray bodies in their surface properties? The two groups have indistinguishable colors and albedos (see Table 4). The Small/Gray bodies cannot be observed to high enough a phase angle, so we do not have measures of  $S_{>5}$  for them. The surge slope at low phase angles ( $S_{\leq}$ ) has good overlap between the Small/Grays and the Trojans, but the Small/Grays appear to go to higher values than the Trojans. The range of  $S_{\leq}$  for all nine of our observed Trojans is -0.01 to 0.09 mag/°. The range of  $S_{\leq}$  for all nine small/gray bodies (8 gray Centaurs and 1 gray SDO) is 0.01-0.18 mag/°. These ranges are comparable, but three of the small/gray bodies lie above the range for the Trojans. The key science question is whether the two distributions of  $S_{\leq}$  are consistent with being drawn from the same parent population. A statistical test to answer this question is the Kolmogorov-Smirnov (K-S) test (Press et al., 1986). We have constructed the cumulative distributions in  $S_{\leq}$  for nine objects in each of the two samples, and we find the largest difference between the two distributions is 0.44. The K-S probability is then that two samples taken from the same parent population will have a difference  $\leq 0.44$  only 25% of the time. This is near a confidence level that corresponds to a Gaussian one-sigma result, and such differences are commonly expected. That is, the two distributions are fairly close and certainly not significantly different. Thus, we conclude that the Schaefer et al. (2008a; 2009b) prediction is confirmed, because the Trojans appear to have a similar distribution of surge properties as the other Small/Gray bodies in our Solar System.

What we are seeing is that all the surface properties of the Trojans are indistinguishable from those of the gray Centaurs, gray SDOs, and dead comet candidates. That is, all four dynamically distinct groups have the same surfaces. This could arise because the bodies are all genetically related, in that they all come from the same parent population and have all arrived at the same end-state (i.e., lost their surface ices) through differing evolutionary paths that leave them with different orbits. Thus, the bodies all formed in the outer Solar System (then appearing as Small/Red bodies), and were later perturbed into orbits that carried them close enough to the Sun for them to lose

their surface ices and be transformed into Small/Gray bodies. Thus, for surface properties, it does not matter whether the ice was lost long ago after capture into a Trojan orbit long ago or whether the ice has been recently lost by a Centaur that is temporarily getting close enough to the Sun.

We can now test the traditional hypothesis that the Trojans formed around the orbit of Jupiter. Again, we only have the imperfect comparison with the D, P, and C class asteroids. The albedos of the Trojans and asteroids are indistinguishable. The B-R colors are similar, even though the Trojans appear to extend to slightly smaller values. But due to limited numbers of Trojans and D class asteroids, this difference in distribution is not significant. The distribution of  $S_{>5}$  is similar for the two groups, but again the small numbers makes for a relatively weak test. For  $S_{\leq 2}$ , the ranges of the two groups are close to each other and with a small overlap. But the P and C class asteroids all have closely identical phase curves (Belskaya and Shevchenko, 2000) with slopes only at the top end of the Trojan range. We have used a K-S test to see if the measured  $S_{\leq 2}$  are consistent with both samples being drawn from the same parent population. Our comparison is between our nine Trojans and the thirteen P and C class asteroids with phase curves in Belskaya and Shevchenko (2000). No D class asteroids in the main belt have measured phase curves. The two cumulative distributions have a maximum difference of 0.79, in that 79% of the Trojans have  $S_{\leq 2} < 0.065 \text{ mag/}^\circ$  while 0% of the P and C asteroids have  $S_{\leq 2} < 0.065 \text{ mag/}^\circ$ . The K-S probability is then that two samples taken from the same parent population will have a difference  $\leq 0.79$  only 0.10% of the time. That is, at the thousand-to-one confidence level, the surge properties of the Trojans and the asteroids are different. This confidence level is substantially stronger than ‘3-sigma’, so we take this as a strong result.

A plausible possibility is that the Trojans have a mixed population, composed of bodies originating from near the orbit of Jupiter and from the outer Solar System. We can use a K-S test to put limits on the fraction of Trojans from a population like the P and C asteroids. At the two-sigma confidence level (95%), we find that no more than one-third of the Trojans can come from the asteroid classes.

With this, we see that the Trojans do not have the same surface properties as the P and C asteroids. Thus, to the extent that the P and C asteroids are representative of the bodies that originally formed around Jupiter’s orbit, we can exclude the Trojans as having come from that population. As such, we have evidence against the traditional view for the formation of the Trojans.

Nevertheless, we are intrigued by the close similarity in surface properties between the Small/Gray bodies and the P and C asteroids. In particular, if we put the P and C types together in one group, their phase slopes, B-R, and albedo distributions are indistinguishable from the small/gray group. We have performed a K-S test to any difference in the surge slope distribution between the 9 Small/Gray bodies and the 13 P and C asteroids. The maximum difference between the cumulative distributions is 0.36, with 44% of the Small/Gray bodies and 8% of the P&C asteroids having  $S_{\leq 2} < 0.075 \text{ mag/}^\circ$ . The K-S probability is 62% of the two samples coming from the same parent

population will have a maximum difference this large. This is saying that the two distributions are indistinguishable. (Note, that for surge slopes, the Trojans and P and C asteroids can both be indistinguishable from the Small/Grays and yet be significantly different from each other.) Viewed on the basis of the surface properties we have examined, the P and C asteroids look exactly like the Small/Gray bodies of the outer Solar System.

Very recently, Levison et al. (2009) have suggested that most of D and P types in the main belt formed in the outer Solar System and were captured, like the Trojans, during an early phase of planetary migration. Our observations that P- and D-type asteroids, Trojans, and small gray bodies from the outer Solar System not only have similar colors and albedos but also similarly flat phase curves supports this conclusion. However, the somewhat different surge slopes between the Trojans and the P and C asteroids suggests that there might be some differences in history or original composition. Within this picture, the large class of Small/Gray bodies (that is, small bodies formed in the outer Solar System that have lost all their surface ices) consists of gray Centaurs, gray SDOs, dead comets, Trojans, D-type asteroids, P-type asteroids, and C-type asteroids.

In summary, we have nine well-measured phase curves, the first for Trojan asteroids. Our phase curves are nearly linear with median slopes of  $0.05 \text{ mag}/^\circ$ . These slopes are too high for the shadow-hiding mechanism of opposition surge, so the coherent-backscattering mechanism must dominate. In a comparison with the Small/Gray bodies (i.e., objects formed in the outer Solar System that have lost their surface ices), we find that the Trojans have a similar distribution of surface properties. This is a fulfillment of a prediction that the Trojan surges would be indistinguishable from the Small/Gray surges. Indeed, we find that the Trojans are indistinguishable from the Small/Gray bodies in all surface properties. In a comparison with all the other classes of bodies (the Small/Red icy bodies, transition bodies, and five main belt asteroid classes), we find that the surge properties are significantly different. This result is evidence against the traditional idea that Trojans formed around the orbit of Jupiter. Overall, our results are in good agreement with the theory that the Trojans are simply de-iced bodies from the outer Solar System (Schaefer et al., 2008b; 2009b) and were captured into their current orbits during the migration of the giant planets (Morbidelli et al., 2005).

## Conclusions

Trojan asteroids can serve as an indicator for the early history of our Solar System, with the Nice model of Morbidelli et al. (2005) claiming that the Trojans were originally formed in the outer Solar System, in contrast to the traditional view that they formed near the orbit of Jupiter. If Trojans can be demonstrated to come from the outer Solar System, then this would lend good support to the details of the migrations of the gas giant planets. One way to test the Nice model is to look at the surface properties of the Trojans in comparison with de-iced bodies from the outer Solar System (including the gray Centaurs and dead comets) and with asteroids from the outer belt (like the P and C

classes). To this end, we are reporting on a program to get well-sampled phase curves of Trojans.

Prior to our work, there was essentially no useful measure of the phase curve of any Trojan asteroid. (After our work, Shevchenko et al. (2009) report a remarkably accurate phase curve for one Trojan, which is in close agreement with our phase curve.) Now, with our work, we have nine good phase curves for comparison with other classes of bodies.

We find that the nine Trojan phase curves are consistent with a simple linear model from phases over the range of roughly  $0.2^\circ$ - $10^\circ$ . The slopes for eight of them are from  $0.04$ - $0.09$  mag/ $^\circ$ . (The ninth Trojan has an unprecedented negative slope of  $-0.02 \pm 0.01$  mag/ $^\circ$ , for which we have no sure explanation.) The average uncertainty in these slopes is  $0.02$  mag/ $^\circ$ , although there could be some extra systematic uncertainty at this level or smaller arising from uncorrected rotational modulations. With these slopes, the coherent backscattering mechanism must be dominating over the shadow hiding mechanism.

We compared the Trojan surface properties (surge slope, albedo, and B-R color) with those of de-iced outer Solar System bodies as well as those of outer main belt asteroids. For the albedo and color parameters, the Trojans are indistinguishable from either group. For the surge slope, the Trojans are indistinguishable from the small/gray bodies, yet are significantly different from the P and C asteroids. Thus, we find support for the idea that the Trojans were formed in the outer Solar System, captured into the Trojan orbit during migration of the giant planets, and then lost their surface ice due to proximity with the Sun.

## **Acknowledgments**

The National Aeronautics and Space Administration provided funds to support this research under grants NAG5-13533 and NAG5-13369.

## References

- Barucci, M. A., Cruikshank, D. P., Mottola, S., Lazzarin, M., Physical properties of Trojan and Centaur asteroids. In: W. F. Bottke, Jr., A. Cellino, P. Paolicchi, R. P. Binzel, (Eds.), Asteroids III. The University of Arizona Press, Tucson, AZ, 2002, pp. 273-287.
- Belskaya, I. N., Shevchenko, V. G., 2000. Opposition effect of asteroids. *Icarus*. 147, 94-105.
- Bendjoya, P., Cellino, A., Di Martino, M., Saba, L., 2004. Spectroscopic observations of Jupiter Trojans. *Icarus*. 168, 374-384.
- Buratti, B. J., Gibson, J., Mosher, J. A., 1992. CCD photometry of the Uranian satellites. *The Astronomical Journal*. 104, 1628-1622.
- Buratti, B. J., Veverka, J., 1985. Photometry of rough planetary surfaces - the role of multiple scattering. *Icarus*. 64, 320-328.
- Chapman, C. R., Gaffey, M. J., Spectral reflectances of the asteroids. In: T. Gehrels, (Ed.), Asteroids. The University of Arizona Press, Tucson, AZ, 1979, pp. 1064-1089.
- Degewij, J., Andersson, L. E., Zellner, B., 1980. Photometric properties of outer planetary satellites. *Icarus*. 44, 520-540.
- Fernandez, Y. R., Sheppard, S. S., Jewitt, D. C., 2003. The albedo distribution of jovian Trojan asteroids. *The Astronomical Journal*. 126, 1563-1574.
- Fornasier, S., Dotto, E., Hainaut, O., Marzari, F., Boehnhardt, H., de Luise, F., Barucci, M. A., 2007. Visible spectroscopic and photometric survey of Jupiter Trojans: Final results on dynamical families. *Icarus*, Volume 190, Issue 2, p. 622-642.

- Fornasier, S., Dotto, E., Marzari, F., Barucci, M. A., Boehnhardt, H., Hainaut, O., de Bergh, C., 2004. Visible spectroscopic and photometric survey of L5 Trojans: Investigation of dynamical families. *Icarus*, Volume 172, Issue 1, p. 221-232.
- French, L. M., 1987. Rotation properties of four L5 Trojan asteroids from CCD photometry. *Icarus*. 72, 325-341.
- Gutierrez-Moreno, A., Moreno, H., Cortes, G., 1986. A study of atmospheric extinction at Cerro Tololo Inter-American observatory. II. *PASP*. 98, 1208-1212.
- Hapke, B., 1993. *Theory of reflectance and emittance spectroscopy*. Cambridge University Press, Cambridge.
- Hapke, B., 2002. Bidirectional reflectance spectroscopy 5. The coherent backscatter opposition effect and anisotropic scattering. *Icarus*. 157, 523-534.
- Helfenstein, P., Veverka, J., Hillier, J., 1997. Lunar opposition effect: A test of alternative models. *icarus*. 128, 2-14.
- Jewitt, D. C., 2002. From Kuiper belt object to cometary nucleus: The missing ultrared matter. *The Astronomical Journal*. 123, 1039-1049.
- Lamy, P., Toth, I., 2009. The colors of cometary nuclei - comparison with other primitive bodies of the solar system and implications for their origin. *Icarus*. 201, 674-713.
- Lamy, P. L., Toth, I., Fernandez, Y. R., Weaver, H. A., The sizes, shapes, albedos, and colors of cometary nuclei. In: M. C. Festou, H. U. Keller, H. A. Weaver, (Eds.), *Comets II*. University of Arizona Press, Tucson, AZ, 2004, pp. 223-264.
- Landolt, A. U., 1992. UBVRI photometric standard stars in the magnitude range  $11.5 < V < 16.0$  around the celestial equator. *The Astronomical Journal*. 104, 340-491.
- Landolt, A. U., 2009. UBVRI photometric standard stars around the celestial equator: Updates and additions. *The Astronomical Journal*. 137, 4186-4269.

- Levison, H. F., Bottke, W. F., Jr., Gounelle, M., Morbidelli, A., Nesvorný, D., Tsiganis, K., 2009. The contamination of the asteroid belt by primordial trans-Neptunian objects. *Nature*, 460, 364-366.
- Molnar, L. A., Haegert, M. J., Hoogeboom, K. M., 2008. Lightcurve analysis of an unbiased sample of Trojan asteroids. *Minor Planet Bulletin*. 35, 82-84.
- Morbidelli, A., Levison, H. F., Tsiganis, K., Gomes, R., 2005. Chaotic capture of Jupiter's Trojan asteroids in the early solar system. *Nature*. 435, 462-465.
- Muironen, K., Piironen, J., Shkuratov, Y. G., Ovcharenko, A., Clark, B. E., Asteroid photometric and polarimetric phase effects. In: W. F. Bottke, Jr., A. Cellino, P. Paolicchi, R. P. Binzel, (Eds.), *Asteroids III*. The University of Arizona Press, Tucson, AZ, 2002, pp. 123-138.
- Press, W. H., Flannery, B. P., Teukolsky, S. A., Vetterling, W. T., 1986. *Numerical recipes, the art of scientific computing*.
- Rabinowitz, D. L., Barkume, K., Brown, M. E., Roe, H., Schwartz, M., Tourtellotte, S. W., Trujillo, C., 2006. Photometric observations constraining the size, shape, and albedo of 2003 EL61, a rapidly rotating, Pluto-sized object in the Kuiper Belt. *Astrophysical Journal*. 639, 1238-1251.
- Rabinowitz, D. L., Schaefer, B. E., Tourtellotte, S. W., 2007. The diverse solar phase curves of distant icy bodies. I. Photometric observations of 18 trans-Neptunian objects, 7 Centaurs, and Nereid. *The Astronomical Journal*. 133, 26-43.
- Roig, F., Ribeiro, A. O., Gil Hutton, R., 2008. Taxonomy of asteroid families among the Jupiter Trojans: Comparison between spectroscopic data and the Sloan Digital Sky Survey colors. *Astronomy and Astrophysics*. 483, 911-931.
- Rufener, F., 1986. Extinction variations at La Silla. *ESO Messenger*. June, 44, 32-35.

- Schaefer, B. E., Rabinowitz, D. L., Tourtellotte, S. W., Division of icy bodies into groups based on surface properties. American Astronomical Society, DPS meeting #40, #47.04, 2008a.
- Schaefer, B. E., Rabinowitz, D. L., Tourtellotte, S. W., 2009a. Division of icy bodies into groups based on surface properties. *Icarus*. in preparation.
- Schaefer, B. E., Rabinowitz, D. L., Tourtellotte, S. W., 2009b. The diverse solar phase curves of distant icy bodies. II. The cause of the opposition surges and their correlations. *The Astronomical Journal*. 137, 129-144.
- Schaefer, M. W., Schaefer, B. E., Rabinowitz, D. L., Tourtellotte, S. W., Phase curves of 10 Trojan asteroids in BVI over a wide phase range. American Astronomical Society, DPS meeting #40, Ithaca, NY, 2008b, pp. 28.13.
- Sheppard, S. S., 2007. Light curves of dwarf Plutonian planets and other large Kuiper belt objects: Their rotations, phase functions, and absolute magnitudes. *The Astronomical Journal*. 134, 787-798.
- Sheppard, S. S., Jewitt, D. C., 2002. Time-resolved photometry of Kuiper belt objects: Rotations, shapes, and phase functions. *The Astronomical Journal*. 124, 1757-1775.
- Shevchenko, V. G., Krugly, Y. N., Belskaya, I. N., Chiorny, V. G., Gaftonyuk, N. M., Slyusarev, I. G., Tereschenko, I. A., Donchev, Z., Ivanova, V., Borisov, G., Ibrahimov, M. A., Marshalkina, A. L., Molotov, I. E., Do Trojan asteroids have the brightness opposition effect? , 40th Lunar and Planetary Science Conference, Vol. 40, Houston, TX, 2009, pp. 1391.
- Stankevich, D. G., Shkuratov, Y. G., Muinonen, K., 1999. Shadow hiding effect in inhomogeneous layered particulate media. *Journal of Quantitative Spectroscopy and Radiative Transfer*. 63, 445-448.
- Stansberry, J., Grundy, W., Brown, M., Cruikshank, D., Spencer, J., Trilling, D., Margot, J.-L., Physical properties of Kuiper belt and Centaur objects: Constraints from the

- spitzer space telescope. In: M. A. Barucci, H. Boehnhardt, D. P. Cruikshank, A. Morbidelli, (Eds.), *The solar system beyond Neptune*. The University of Arizona Press, Tucson, AZ, 2008, pp. 161-179.
- Tegler, S. C., Romanishin, W., Consolmagno, G. J., 2003. Color patterns in the Kuiper Belt: A possible primordial origin. *The Astrophysical Journal*. 599, L49-L52.
- Verbiscer, A. J., French, R. G., McGhee, C. A., 2005. The opposition surge of enceladus. *Icarus*. 173, 66-83.
- Zellner, B., Asteroid taxonomy and the distribution of the compositional types. In: T. Gehrels, (Ed.), *Asteroids*. The University of Arizona Press, Tucson, AZ, 1979, pp. 783-806.

**Table 1. Summary of Observations**

<b>Number</b>	<b>Name</b>	<b>Group</b>	<b>H (mag)</b>	<b>i (°)</b>	<b>Dates observed</b>	<b>Phase range(°)</b>	<b># obs.</b>
588	Achilles	Greek/L4	8.67	10.32	2007 July 12-Sep 30	0.165-8.202	119
1208	Troilus	Trojan/L5	8.99	33.56	2008 May 5-May 24	0.199-3.247	35
4348	Poulydamas	Trojan/L5	9.20	7.96	2008 Mar 22-May 13	0.207-6.821	26
6998	Tithonus	Trojan/L5	11.30	1.73	2008 Apr 11-May 10	0.052-4.576	31
8317	Eurysaces	Greek/L4	10.70	0.95	2006 Jun 13-2007 Oct 2	0.132-11.067	228
12126	(1999 RM11)	Trojan/L5	10.10	2.04	2008 Mar 26-May 6	0.173-7.096	40
13323	(1998 SQ)	Greek/L4	10.70	0.91	2007 Mar 21-Oct 2	0.349-10.33	91
24506	(2001 BS15)	Greek/L4	10.50	11.82	2007 July 12-Sep 29	0.136-8.651	119
51378	(2001 AT33)	Greek/L4	11.10	33.63	2007 July 11-Oct 2	0.214-10.28	114

Table 2.

## (a) 588 Achilles

JD (B)	JD (V)	JD (I)	B	$\sigma_B$	V	$\sigma_V$	I	$\sigma_I$	B <sub>red</sub>	V <sub>red</sub>	I <sub>red</sub>	Phase
4293.8445	4293.8465	...	16.646	0.013	15.904	0.008	...	...	9.502	8.760	...	5.584
4295.8272	4295.8292	4295.8311	16.657	0.007	15.889	0.005	14.946	0.010	9.521	8.753	7.810	5.266
4309.7259	4309.7279	4309.7298	16.431	0.043	15.620	0.023	14.672	0.031	9.345	8.534	7.586	2.826
4315.7208	4315.7228	4315.7247	16.420	0.013	15.610	0.011	14.684	0.016	9.347	8.537	7.611	1.691
4316.7279	4316.7299	4316.7318	16.336	0.018	15.560	0.005	14.705	0.009	9.265	8.489	7.634	1.497
4319.7276	4319.7296	4319.7315	16.326	0.006	15.549	0.004	14.657	0.004	9.260	8.483	7.591	0.916
4320.5518	4320.5538	4320.5557	16.253	0.007	15.551	0.005	14.664	0.010	9.188	8.486	7.599	0.756
4320.8455	4320.8475	4320.8494	16.268	0.008	15.543	0.007	14.677	0.009	9.203	8.478	7.612	0.699
4322.8415	4322.8435	4322.8454	16.228	0.009	15.548	0.011	14.590	0.006	9.165	8.485	7.527	0.315
4323.6699	4323.6721	4323.6742	16.292	0.048	15.548	0.041	14.634	0.018	9.230	8.486	7.572	0.165
4325.6666	4325.6686	4325.6705	16.308	0.008	15.541	0.007	14.624	0.009	9.247	8.480	7.563	0.264
4325.8304	4325.8323	4325.8343	16.261	0.010	15.547	0.010	14.608	0.010	9.200	8.486	7.547	0.295
4326.5248	4326.5270	4326.5291	16.296	0.008	15.530	0.006	14.651	0.012	9.235	8.469	7.590	0.427
4326.7984	4326.8003	4326.8023	16.248	0.010	15.513	0.009	14.661	0.018	9.187	8.452	7.600	0.480
4327.7919	4327.7939	4327.7958	16.355	0.016	15.626	0.019	14.738	0.019	9.294	8.565	7.677	0.672
4329.5381	4329.5401	4329.5421	16.267	0.007	15.536	0.005	14.779	0.004	9.207	8.476	7.719	1.012
4329.8096	4329.8116	4329.8135	16.272	0.007	15.546	0.007	14.776	0.009	9.212	8.486	7.716	1.065
4330.5588	4330.5607	4330.5627	16.260	0.007	15.533	0.005	14.666	0.007	9.199	8.472	7.605	1.210
4330.8044	4330.8063	4330.8083	16.329	0.006	15.647	0.006	14.795	0.005	9.268	8.586	7.734	1.258
4331.7645	4331.7665	4331.7685	16.317	0.006	15.607	0.006	14.707	0.010	9.256	8.546	7.646	1.444
4332.7703	4332.7722	4332.7741	16.368	0.022	15.615	0.018	14.691	0.013	9.307	8.554	7.630	1.639
4332.8366	4332.8386	4332.8405	16.315	0.050	15.536	0.037	14.657	0.023	9.254	8.475	7.596	1.652
4333.6676	4333.6696	4333.6715	16.355	0.005	15.633	0.004	14.733	0.019	9.293	8.571	7.671	1.812
4334.7252	4334.7272	4334.7291	16.399	0.007	15.660	0.006	14.766	0.030	9.336	8.597	7.703	2.016
4335.7036	4335.7056	4335.7075	16.377	0.009	15.606	0.006	14.682	0.006	9.313	8.542	7.618	2.203
4336.6460	4336.6480	4336.6499	16.360	0.008	15.562	0.011	14.638	0.016	9.295	8.497	7.573	2.383
4340.7052	4340.7072	4340.7092	16.470	0.050	15.780	0.049	14.930	0.014	9.400	8.710	7.860	3.146
4341.7061	4341.7081	4341.7101	16.440	0.012	15.663	0.009	14.700	0.014	9.368	8.591	7.628	3.332
4342.7469	4342.7489	4342.7508	16.605	0.014	15.805	0.012	14.899	0.013	9.531	8.731	7.825	3.523
4344.7438	4344.7459	4344.7478	16.439	0.012	15.724	0.006	14.863	0.008	9.361	8.646	7.785	3.885
4346.6986	4346.7006	4346.7025	16.425	0.017	15.685	0.027	14.766	0.031	9.343	8.603	7.684	4.234
4349.6979	4349.6999	4349.7018	16.549	0.008	15.805	0.005	14.877	0.008	9.459	8.715	7.787	4.757
4351.7302	4351.7322	4351.7341	16.474	0.007	15.768	0.005	14.800	0.023	9.379	8.673	7.704	5.102
4353.7300	4353.7320	4353.7339	16.547	0.008	15.814	0.009	14.878	0.005	9.445	8.712	7.776	5.433
4355.7561	4355.7581	4355.7601	16.620	0.038	15.866	0.043	14.986	0.042	9.512	8.758	7.878	5.760
4357.6853	4357.6873	4357.6893	16.554	0.008	15.826	0.005	14.972	0.005	9.439	8.711	7.857	6.062
4359.6567	4359.6587	4359.6607	16.563	0.008	15.840	0.008	14.905	0.009	9.440	8.717	7.782	6.362
4363.6516	4363.6536	4363.6555	16.622	0.008	15.912	0.007	15.008	0.007	9.483	8.773	7.869	6.941
4371.6303	4371.6323	4371.6343	16.725	0.009	16.051	0.006	15.077	0.009	9.551	8.877	7.903	7.969
4373.6526	4373.6546	4373.6565	16.735	0.007	15.997	0.005	15.066	0.006	9.551	8.813	7.882	8.202

**(b) 1208 Troilus**

<b>JD (B)</b>	<b>JD (V)</b>	<b>JD (I)</b>	<b>B</b>	$\sigma_B$	<b>V</b>	$\sigma_V$	<b>I</b>	$\sigma_I$	<b>B<sub>red</sub></b>	<b>V<sub>red</sub></b>	<b>I<sub>red</sub></b>	<b>Phase</b>
4591.7622	4591.7642	4591.7663	16.681	0.013	15.989	0.007	15.265	0.006	9.793	9.101	8.377	0.625
...	4592.7398	4592.7419	...	...	16.060	0.006	15.307	0.017	...	9.173	8.420	0.427
4593.5733	4593.5753	4593.5774	16.728	0.007	15.984	0.005	15.255	0.005	9.841	9.097	8.368	0.264
4595.5365	4595.5386	4595.5406	16.597	0.107	15.928	0.005	15.170	0.005	9.712	9.043	8.285	0.199
4596.5263	4596.5283	4596.5304	16.712	0.006	15.994	0.005	15.251	0.005	9.827	9.109	8.366	0.387
4596.7865	4596.7885	4596.7906	16.772	0.015	16.073	0.005	15.201	0.006	9.887	9.188	8.316	0.439
4598.5141	4598.5161	4598.5181	16.679	0.015	15.974	0.008	15.208	0.013	9.795	9.090	8.324	0.791
4598.7825	4598.7845	4598.7866	16.670	0.009	15.977	0.006	15.207	0.005	9.786	9.093	8.323	0.846
4599.5063	4599.5083	4599.5103	16.797	0.009	16.048	0.009	15.292	0.013	9.913	9.164	8.408	0.995
4599.8075	4599.8095	4599.8116	16.779	0.012	16.012	0.010	15.240	0.014	9.895	9.128	8.356	1.057
4601.6080	4601.6100	4601.6121	16.750	0.006	16.101	0.005	15.326	0.006	9.865	9.216	8.441	1.426
4610.6473	4610.6493	4610.6514	16.812	0.008	16.123	0.008	15.379	0.010	9.918	9.229	8.485	3.247

**(c) 4348 Poulydamas**

<b>JD (B)</b>	<b>JD (V)</b>	<b>JD (I)</b>	<b>B</b>	$\sigma_B$	<b>V</b>	$\sigma_V$	<b>I</b>	$\sigma_I$	<b>B<sub>red</sub></b>	<b>V<sub>red</sub></b>	<b>I<sub>red</sub></b>	<b>Phase</b>
4547.8036	4547.8056	4547.8077	18.228	0.028	17.540	0.017	16.725	0.018	10.961	10.273	9.458	6.821
4574.6735	4574.6755	4574.6776	17.866	0.016	17.179	0.012	16.430	0.011	10.699	10.012	9.263	2.438
4579.6968	4579.6988	4579.7009	17.599	0.012	16.954	0.012	16.234	0.009	10.441	9.796	9.076	1.493
4580.7074	4580.7094	4580.7115	17.599	0.042	17.017	0.046	16.219	0.037	10.442	9.860	9.062	1.300
4588.5336	4588.5356	4588.5377	17.517	0.011	16.961	0.009	16.167	0.010	10.366	9.810	9.016	0.207
4591.7355	4591.7375	4591.7396	17.679	0.009	16.987	0.007	16.218	0.008	10.528	9.836	9.067	0.824
...	4592.7120	4592.7140	...	...	16.971	0.010	16.173	0.011	...	9.819	9.021	1.012
4593.6761	4593.6781	4593.6802	17.929	0.018	17.176	0.011	16.387	0.013	10.777	10.024	9.235	1.197
4599.6463	4599.6483	4599.6504	18.011	0.012	17.260	0.010	16.482	0.011	10.853	10.102	9.324	2.330

**(d) 6998 Tithonus**

<b>JD (B)</b>	<b>JD (V)</b>	<b>JD (I)</b>	<b>B</b>	$\sigma_B$	<b>V</b>	$\sigma_V$	<b>I</b>	$\sigma_I$	<b>B<sub>red</sub></b>	<b>V<sub>red</sub></b>	<b>I<sub>red</sub></b>	<b>Phase</b>
4567.7462	4567.7482	4567.7502	19.138	0.020	18.385	0.017	17.492	0.018	12.491	11.738	10.845	1.519
4569.5657	4569.5677	4569.5698	19.044	0.040	18.380	0.030	17.456	0.027	12.400	11.736	10.812	1.129
4569.7751	4569.7771	4569.7792	19.095	0.035	18.354	0.033	17.487	0.027	12.451	11.710	10.843	1.084
4574.5267	4574.5288	4574.5308	19.089	0.097	18.250	0.061	17.370	0.042	12.450	11.611	10.731	0.075
4574.8414	4574.8434	4574.8455	19.113	0.088	18.244	0.076	17.485	0.062	12.474	11.605	10.846	0.052
4579.5537	...	...	19.321	0.062	...	...	...	...	12.684	...	...	1.032
4579.8146	4579.8167	4579.8188	19.182	0.069	18.408	0.044	17.608	0.035	12.545	11.771	10.971	1.089
4580.6688	4580.6708	4580.6729	19.265	0.044	18.532	0.040	17.625	0.022	12.627	11.894	10.987	1.273
4588.6044	4588.6064	4588.6085	19.258	0.025	18.551	0.021	17.576	0.031	12.613	11.906	10.931	2.958
4591.5859	4591.5880	4591.5900	19.382	0.023	18.614	0.018	17.630	0.018	12.732	11.964	10.980	3.574
4596.5898	4596.5918	4596.5939	19.404	0.022	18.578	0.017	17.635	0.018	12.743	11.917	10.974	4.576

## (e) 8317 Eurysaces

JD (B)	JD (V)	JD (I)	B	$\sigma_B$	V	$\sigma_V$	I	$\sigma_I$	B <sub>red</sub>	V <sub>red</sub>	I <sub>red</sub>	Phase
3899.8754	...	...	19.542	0.141	...	...	...	...	12.783	...	...	10.377
3899.8782	3899.8809	3899.8823	19.349	0.113	18.595	0.119	17.777	0.110	12.590	11.836	11.018	10.377
3900.8715	...	...	19.521	0.063	...	...	...	...	12.768	...	...	10.287
3900.8742	3900.8770	3900.8784	19.527	0.061	18.733	0.062	17.768	0.048	12.774	11.980	11.015	10.287
3901.8312	...	...	19.162	0.102	...	...	...	...	12.416	...	...	10.198
3901.8339	3901.8367	3901.8381	19.206	0.110	18.480	0.104	17.973	0.147	12.460	11.734	11.227	10.198
3903.8343	...	...	19.367	0.061	...	...	...	...	12.634	...	...	10.003
3903.8370	3903.8398	3903.8412	19.468	0.067	18.572	0.076	17.711	0.075	12.735	11.839	10.978	10.003
3905.7776	...	...	19.437	0.036	...	...	...	...	12.716	...	...	9.801
3905.7803	3905.7831	3905.7845	19.413	0.032	18.623	0.044	17.896	0.054	12.692	11.902	11.175	9.801
3907.7848	...	...	19.391	0.025	...	...	...	...	12.683	...	...	9.580
3907.7875	3907.7903	3907.7917	19.388	0.024	18.698	0.037	17.785	0.045	12.680	11.990	11.077	9.579
3909.8098	...	...	19.457	0.024	...	...	...	...	12.762	...	...	9.343
3909.8125	3909.8152	3909.8166	19.473	0.024	18.817	0.039	17.902	0.038	12.778	12.122	11.207	9.343
3912.8506	...	...	19.293	0.023	...	...	...	...	12.616	...	...	8.963
3912.8533	3912.8560	3912.8574	19.254	0.021	18.538	0.032	17.662	0.035	12.577	11.861	10.985	8.963
3916.8480	...	...	19.172	0.031	...	...	...	...	12.519	...	...	8.420
3916.8507	3916.8535	3916.8549	19.144	0.032	18.529	0.064	17.678	0.055	12.491	11.876	11.025	8.420
3935.7560	...	...	19.120	0.025	...	...	...	...	12.556	...	...	5.238
3935.7587	3935.7615	3935.7629	19.153	0.022	18.416	0.038	17.554	0.034	12.589	11.852	10.990	5.237
3937.7593	...	...	19.100	0.018	...	...	...	...	12.543	...	...	4.849
3937.7620	3937.7648	3937.7662	19.111	0.020	18.280	0.027	17.377	0.028	12.554	11.723	10.820	4.849
3945.7493	...	...	18.993	0.024	...	...	...	...	12.459	...	...	3.226
3945.7520	3945.7548	3945.7562	19.023	0.023	18.206	0.029	17.340	0.029	12.489	11.672	10.806	3.226
3951.8935	...	...	18.525	0.154	...	...	...	...	12.002	...	...	1.920
3951.8935	3951.8935	3951.8935	18.674	0.126	18.053	0.148	17.088	0.084	12.151	11.530	10.565	1.920
3958.7068	...	...	18.691	0.041	...	...	...	...	12.173	...	...	0.474
3958.7095	3958.7122	3958.7136	18.601	0.043	17.986	0.049	17.066	0.042	12.083	11.468	10.548	0.474
3960.7681	...	...	18.609	0.023	...	...	...	...	12.091	...	...	0.225
3960.7708	3960.7736	3960.7750	18.698	0.024	17.980	0.030	17.116	0.027	12.180	11.462	10.598	0.225
3964.7720	...	...	18.623	0.030	...	...	...	...	12.103	...	...	0.940
3964.7747	3964.7775	3964.7789	18.636	0.028	17.874	0.023	16.989	0.026	12.116	11.354	10.469	0.941
3966.7712	...	...	18.640	0.017	...	...	...	...	12.119	...	...	1.369
3966.7740	3966.7767	3966.7781	18.632	0.017	17.853	0.024	17.100	0.025	12.111	11.332	10.579	1.370
3968.7893	...	...	18.764	0.018	...	...	...	...	12.240	...	...	1.804
3968.7921	3968.7948	3968.7962	18.824	0.018	17.990	0.026	17.059	0.028	12.300	11.466	10.535	1.804
3975.7384	...	...	18.892	0.019	...	...	...	...	12.355	...	...	3.279
3975.7411	3975.7439	3975.7453	18.840	0.020	18.071	0.034	17.203	0.031	12.302	11.533	10.665	3.280
3998.6164	...	...	19.275	0.025	...	...	...	...	12.646	...	...	7.528
3998.6191	3998.6219	3998.6233	19.232	0.025	18.446	0.034	17.597	0.038	12.603	11.817	10.968	7.528
4292.8440	...	...	19.463	0.043	...	...	...	...	12.613	...	...	11.067
4292.8467	...	4292.8507	19.518	0.044	...	...	17.887	0.079	12.668	...	11.037	11.066
4310.8524	4310.8564	...	19.262	0.061	18.595	0.044	...	...	12.528	11.861	...	9.499
4316.8476	...	...	19.250	0.039	...	...	...	...	12.551	...	...	8.748

## (e)(cont.) 8317 Eurysaces

JD (B)	JD (V)	JD (I)	B	$\sigma_B$	V	$\sigma_V$	I	$\sigma_I$	B <sub>red</sub>	V <sub>red</sub>	I <sub>red</sub>	Phase
4316.8502	4316.8529	4316.8543	19.236	0.044	18.464	0.049	17.627	0.044	12.537	11.765	10.928	8.748
4331.8552	...	...	19.088	0.022	...	...	...	...	12.463	...	...	6.394
4331.8579	4331.8606	4331.8619	19.146	0.022	18.368	0.038	17.432	0.041	12.522	11.744	10.808	6.393
4331.8661	...	...	19.096	0.024	...	...	...	...	12.472	...	...	6.392
4331.8688	4331.8715	4331.8728	19.119	0.025	18.367	0.037	17.440	0.038	12.495	11.743	10.816	6.391
4333.7448	...	...	18.986	0.019	...	...	...	...	12.369	...	...	6.054
4333.7475	4333.7502	4333.7515	19.029	0.026	18.270	0.028	17.382	0.032	12.412	11.653	10.765	6.053
4335.8654	...	...	19.102	0.028	...	...	...	...	12.493	...	...	5.662
4335.8681	4335.8708	4335.8721	19.089	0.030	18.262	0.045	17.449	0.041	12.480	11.653	10.840	5.662
4338.7836	4338.7876	4338.7856	19.084	0.055	18.268	0.035	17.419	0.027	12.486	11.670	10.821	5.106
4339.8521	4339.8562	4339.8542	18.827	0.067	18.317	0.045	17.278	0.236	12.232	11.722	10.683	4.898
4340.7436	4340.7476	4340.7456	18.860	0.095	18.140	0.046	17.349	0.052	12.268	11.548	10.757	4.723
4345.8049	...	...	18.920	0.031	...	...	...	...	12.342	...	...	3.701
4345.8075	4345.8102	4345.8116	18.885	0.030	18.187	0.038	17.378	0.034	12.307	11.609	10.800	3.700
4348.7449	...	...	18.828	0.020	...	...	...	...	12.256	...	...	3.088
4348.7476	4348.7503	4348.7516	18.822	0.016	18.075	0.025	17.252	0.032	12.250	11.503	10.680	3.087
4350.8353	4350.8394	4350.8374	18.940	0.024	18.147	0.020	17.312	0.019	12.372	11.579	10.744	2.645
4351.7786	4351.7826	4351.7806	18.755	0.023	18.139	0.020	17.308	0.018	12.188	11.572	10.741	2.443
4352.8022	4352.8063	4352.8043	18.964	0.038	18.159	0.021	17.297	0.030	12.398	11.593	10.731	2.223
4353.7999	4353.8040	4353.8020	18.719	0.038	18.034	0.034	17.142	0.032	12.155	11.470	10.578	2.008
4354.8471	4354.8511	4354.8491	18.813	0.025	18.108	0.021	17.253	0.045	12.250	11.545	10.690	1.782
4355.8013	4355.8054	4355.8034	18.659	0.019	17.927	0.015	17.016	0.019	12.097	11.365	10.454	1.575
4356.7567	...	...	18.755	0.022	...	...	...	...	12.193	...	...	1.367
4356.7593	4356.7620	4356.7634	18.730	0.020	18.047	0.033	17.256	0.025	12.168	11.485	10.694	1.367
4357.7522	...	...	18.687	0.016	...	...	...	...	12.126	...	...	1.151
4357.7548	4357.7575	4357.7588	18.702	0.015	17.935	0.024	17.172	0.024	12.141	11.374	10.611	1.150
4358.5742	...	...	18.616	0.024	...	...	...	...	12.055	...	...	0.972
4358.5769	4358.5796	4358.5810	18.627	0.021	18.027	0.035	17.257	0.033	12.066	11.466	10.696	0.971
4358.8000	...	...	18.641	0.022	...	...	...	...	12.080	...	...	0.923
4358.8027	4358.8054	4358.8067	18.592	0.022	17.881	0.029	17.175	0.030	12.031	11.320	10.614	0.922
4359.5559	...	...	18.473	0.031	...	...	...	...	11.912	...	...	0.759
4359.5586	4359.5613	4359.5626	18.495	0.036	17.940	0.032	17.000	0.037	11.934	11.379	10.439	0.758
4359.7985	...	...	18.513	0.025	...	...	...	...	11.952	...	...	0.706
4359.8011	4359.8038	4359.8052	18.658	0.024	17.949	0.035	17.134	0.045	12.097	11.388	10.573	0.705
4360.6728	...	...	18.649	0.037	...	...	...	...	12.089	...	...	0.518
4360.8412	...	...	18.704	0.028	...	...	...	...	12.144	...	...	0.482
4360.8439	4360.8466	4360.8480	18.678	0.026	17.989	0.036	17.223	0.040	12.118	11.429	10.663	0.482
4361.6509	4361.6550	4361.6530	18.701	0.027	17.974	0.025	17.076	0.024	12.141	11.414	10.516	0.314
4361.8054	4361.8095	4361.8075	18.756	0.026	18.015	0.023	17.175	0.023	12.195	11.454	10.614	0.283
4362.5619	4362.5660	4362.5640	18.565	0.028	17.957	0.025	17.024	0.026	12.004	11.396	10.463	0.153
4362.7682	4362.7723	4362.7702	18.547	0.027	18.014	0.031	17.106	0.026	11.986	11.453	10.545	0.132
4363.5534	4363.5574	4363.5554	18.709	0.177	18.018	0.041	16.975	0.106	12.148	11.457	10.414	0.181
4363.7295	4363.7336	4363.7316	18.698	0.030	18.107	0.022	17.173	0.023	12.137	11.546	10.612	0.211
4364.5818	4364.5859	4364.5838	18.675	0.044	18.077	0.030	17.206	0.025	12.113	11.515	10.644	0.378

## (e)(cont.) 8317 Eurysaces

JD (B)	JD (V)	JD (I)	B	$\sigma_B$	V	$\sigma_V$	I	$\sigma_I$	B <sub>red</sub>	V <sub>red</sub>	I <sub>red</sub>	Phase
4365.5468	4365.5509	4365.5488	18.713	0.100	18.029	0.059	17.105	0.085	12.151	11.467	10.543	0.583
4366.8067	...	4366.8087	18.601	0.088	...	...	17.155	0.040	12.038	...	10.592	0.855
4367.5424	4367.5465	4367.5444	18.604	0.060	18.058	0.039	17.197	0.033	12.040	11.494	10.633	1.014
4367.7876	4367.7916	4367.7896	19.071	0.184	18.121	0.084	17.258	0.095	12.507	11.557	10.694	1.067
4368.8051	4368.8092	4368.8071	18.646	0.137	18.089	0.104	17.102	0.064	12.080	11.523	10.536	1.288
4371.7150	...	...	18.641	0.048	...	...	...	...	12.071	...	...	1.918
4371.7177	4371.7205	4371.7218	18.216	0.236	18.016	0.061	17.118	0.041	11.646	11.446	10.548	1.918
4372.7473	...	...	18.594	0.030	...	...	...	...	12.022	...	...	2.139
4372.7499	4372.7527	4372.7540	18.704	0.049	17.985	0.047	17.149	0.036	12.132	11.413	10.577	2.140
4372.7572	...	...	18.795	0.034	...	...	...	...	12.223	...	...	2.142
4372.7598	4372.7626	4372.7640	18.786	0.035	18.097	0.039	17.227	0.031	12.214	11.525	10.655	2.142
4373.7274	...	...	18.842	0.031	...	...	...	...	12.268	...	...	2.349
4373.7301	4373.7328	4373.7342	18.824	0.032	18.081	0.032	17.246	0.030	12.250	11.507	10.672	2.350
4374.7895	...	...	18.772	0.067	...	...	...	...	12.196	...	...	2.575
4374.7922	4374.7949	4374.7963	18.821	0.094	18.108	0.075	17.234	0.057	12.245	11.532	10.658	2.576
4375.6841	...	...	18.918	0.028	...	...	...	...	12.340	...	...	2.765
4375.6867	4375.6895	4375.6908	18.985	0.034	18.063	0.044	17.308	0.045	12.407	11.485	10.730	2.765

## (f) 12126 (1999 RM11)

JD (B)	JD (V)	JD (I)	B	$\sigma_B$	V	$\sigma_V$	I	$\sigma_I$	B <sub>red</sub>	V <sub>red</sub>	I <sub>red</sub>	Phase
4551.7874	4551.7895	4551.7915	17.955	0.022	17.272	0.030	16.390	0.019	11.173	10.490	9.608	0.956
4554.6254	4554.6274	4554.6295	17.977	0.014	17.289	0.010	16.332	0.011	11.201	10.513	9.556	0.379
4554.8191	4554.8211	4554.8232	17.999	0.014	17.320	0.013	16.427	0.017	11.223	10.544	9.651	0.342
4555.5536	4555.5556	4555.5576	17.847	0.012	17.153	0.011	16.236	0.010	11.072	10.378	9.461	0.216
4555.8399	4555.8420	4555.8440	17.911	0.017	17.238	0.011	16.339	0.012	11.137	10.464	9.565	0.180
4556.5877	4556.5897	4556.5918	17.845	0.011	17.231	0.009	16.331	0.011	11.072	10.458	9.558	0.173
4556.7671	4556.7691	4556.7711	18.020	0.011	17.334	0.009	16.415	0.009	11.247	10.561	9.642	0.191
4557.5428	4557.5448	4557.5468	17.770	0.013	17.101	0.017	16.197	0.012	10.998	10.329	9.425	0.315
4557.8198	4557.8218	4557.8239	17.956	0.013	17.249	0.017	16.318	0.010	11.185	10.478	9.547	0.367
4559.5405	4559.5425	4559.5446	17.790	0.013	17.268	0.014	16.180	0.027	11.021	10.499	9.411	0.714
4559.8295	4559.8315	4559.8335	17.961	0.013	17.357	0.011	16.357	0.020	11.192	10.588	9.588	0.774
4569.7281	4569.7302	4569.7322	17.943	0.012	17.274	0.010	16.358	0.010	11.177	10.508	9.592	2.835
4580.6337	4580.6357	4580.6378	18.122	0.018	17.394	0.019	16.487	0.017	11.342	10.614	9.707	4.989
...	...	4592.6605	...	...	...	...	16.787	0.012	...	...	9.974	7.096

## (g) 13323 (1998 SQ)

JD (B)	JD (V)	JD (I)	B	$\sigma_B$	V	$\sigma_V$	I	$\sigma_I$	B <sub>red</sub>	V <sub>red</sub>	I <sub>red</sub>	Phase
4180.8705	...	...	20.089	0.081	...	...	...	...	12.496	...	...	9.362
4180.8725	4180.8744	4180.8764	20.073	0.078	19.213	0.058	18.431	0.063	12.480	11.620	10.838	9.362
4191.8325	4191.8344	4191.8364	19.840	0.262	19.085	0.119	18.436	0.110	12.311	11.556	10.907	9.975
4192.8612	...	...	19.776	0.161	...	...	18.411	0.066	12.254	...	...	10.019
4192.8631	4192.8651	4192.8671	19.923	0.167	19.318	0.110	18.411	0.066	12.401	11.796	10.889	10.020
4193.8647	4193.8667	4193.8687	19.917	0.161	19.277	0.095	18.383	0.062	12.401	11.761	10.867	10.061
...	4194.8705	...	...	...	19.189	0.078	...	...	...	11.679	...	10.099
...	4194.8724	4194.8744	...	...	19.165	0.078	18.293	0.055	...	11.655	10.783	10.100
...	4196.8782	...	...	...	19.431	0.080	...	...	...	11.934	...	10.170
...	4196.8802	4196.8822	...	...	19.257	0.067	18.601	0.069	...	11.760	11.104	10.170
...	4197.8703	...	...	...	19.294	0.064	...	...	...	11.803	...	10.202
...	4197.8723	4197.8743	...	...	19.345	0.061	18.332	0.051	...	11.854	10.841	10.202
...	4198.8693	...	...	...	19.247	0.058	...	...	...	11.762	...	10.231
...	4198.8712	4198.8732	...	...	19.188	0.054	18.475	0.057	...	11.703	10.990	10.231
...	4216.7947	...	...	...	19.097	0.033	...	...	...	11.730	...	10.330
...	4216.7967	4216.7987	...	...	19.082	0.036	18.253	0.036	...	11.715	10.886	10.330
...	4219.9127	...	...	...	19.051	0.032	...	...	...	11.705	...	10.260
...	4219.9147	4219.9167	...	...	19.054	0.031	18.243	0.034	...	11.708	10.897	10.260
...	4257.8482	...	...	...	18.909	0.061	...	...	...	11.800	...	7.140
...	4257.8502	4257.8522	...	...	18.860	0.065	17.999	0.063	...	11.751	10.890	7.140
...	4277.8159	...	...	...	18.460	0.022	...	...	...	11.436	...	3.942
...	4277.8179	4277.8199	...	...	18.488	0.022	17.623	0.023	...	11.464	10.599	3.942
4293.8161	...	...	19.054	0.024	...	...	...	...	12.064	...	...	0.909
4293.8181	4293.8201	4293.8221	19.064	0.023	18.329	0.020	17.551	0.021	12.074	11.339	10.561	0.908
...	4295.8227	...	...	...	18.344	0.018	...	...	...	11.356	...	0.528
...	4295.8246	4295.8267	...	...	18.312	0.018	17.518	0.021	...	11.324	10.530	0.527
...	4295.8455	...	...	...	18.278	0.019	...	...	...	11.290	...	0.523
...	4295.8474	4295.8494	...	...	18.334	0.020	17.533	0.022	...	11.346	10.545	0.523
...	4296.8077	...	...	...	18.281	0.018	...	...	...	11.293	...	0.353
...	4296.8097	4296.8117	...	...	18.266	0.018	17.500	0.019	...	11.278	10.512	0.352
...	4296.8255	...	...	...	18.256	0.018	...	...	...	11.268	...	0.350
...	4296.8274	4296.8295	...	...	18.262	0.020	17.439	0.017	...	11.274	10.451	0.349
...	4300.7132	...	...	...	18.380	0.021	...	...	...	11.394	...	0.514
...	4300.7152	4300.7172	...	...	18.390	0.021	17.533	0.023	...	11.404	10.547	0.514
...	4300.7408	...	...	...	18.261	0.019	...	...	...	11.275	...	0.519
...	4300.7427	4300.7448	...	...	18.311	0.021	17.443	0.024	...	11.325	10.457	0.519
4301.7610	...	...	19.077	0.023	...	...	...	...	12.091	...	...	0.711
4301.7630	4301.7650	4301.7670	19.055	0.023	18.308	0.018	17.526	0.021	12.069	11.322	10.540	0.712
4301.7849	...	...	19.064	0.024	...	...	...	...	12.078	...	...	0.715
4301.7869	4301.7889	4301.7909	19.021	0.022	18.314	0.020	17.495	0.022	12.035	11.328	10.509	0.716
4304.7512	...	...	18.998	0.035	...	...	...	...	12.010	...	...	1.289
4304.7531	4304.7551	4304.7571	19.014	0.034	18.265	0.027	17.503	0.028	12.026	11.277	10.515	1.290
4305.7426	...	...	18.859	0.053	...	...	...	...	11.871	...	...	1.482
4305.7445	4305.7465	...	18.824	0.054	18.040	0.041	...	...	11.836	11.052	...	1.483

**(g)(cont.) 13323 (1998 SQ)**

<b>JD (B)</b>	<b>JD (V)</b>	<b>JD (I)</b>	<b>B</b>	$\sigma_B$	<b>V</b>	$\sigma_V$	<b>I</b>	$\sigma_I$	<b>B<sub>red</sub></b>	<b>V<sub>red</sub></b>	<b>I<sub>red</sub></b>	<b>Phase</b>
4307.7410	...	...	19.120	0.041	...	...	...	...	12.130	...	...	1.870
4307.7430	4307.7450	4307.7471	19.107	0.043	18.430	0.030	17.541	0.027	12.117	11.440	10.551	1.871
...	4308.6800	...	...	...	18.389	0.029	...	...	...	11.398	...	2.052
...	4308.6819	4308.6839	...	...	18.414	0.033	17.610	0.032	...	11.423	10.619	2.052
...	4339.7266	...	...	...	18.785	0.088	...	...	...	11.700	...	7.314
...	4339.7286	4339.7307	...	...	18.616	0.077	17.851	0.064	...	11.531	10.766	7.314
...	4372.5875	...	...	...	19.137	0.046	...	...	...	11.868	...	10.207
...	4372.5895	4372.5915	...	...	19.067	0.044	18.226	0.040	...	11.798	10.957	10.207
...	4375.5717	...	...	...	18.992	0.056	...	...	...	11.705	...	10.311
...	4375.5737	4375.5758	...	...	19.024	0.066	18.139	0.083	...	11.737	10.852	10.311

## (h) 24506 (2001 BS15)

JD (B)	JD (V)	JD (I)	B	$\sigma_B$	V	$\sigma_V$	I	$\sigma_I$	B <sub>red</sub>	V <sub>red</sub>	I <sub>red</sub>	Phase
4293.8571	...	4293.8611	19.376	0.030	...	...	17.671	0.022	12.339	...	10.634	8.651
4315.7736	4315.7755	4315.7776	18.866	0.078	18.221	0.053	17.356	0.041	11.938	11.293	10.428	5.499
4319.7588	4319.7607	4319.7627	19.077	0.022	18.286	0.018	17.334	0.017	12.164	11.373	10.421	4.799
...	4325.7825	4325.7847	...	...	18.008	0.069	17.079	0.081	...	11.113	10.184	3.683
4329.7708	4329.7728	4329.7748	18.814	0.130	18.073	0.125	17.238	0.144	11.929	11.188	10.353	2.912
4331.8434	4331.8454	4331.8474	18.857	0.026	18.101	0.021	17.135	0.023	11.976	11.220	10.254	2.504
...	4334.7534	4334.7554	...	...	18.058	0.017	17.119	0.019	...	11.182	10.243	1.924
4336.7192	4336.7212	4336.7232	18.743	0.052	18.142	0.034	17.002	0.024	11.869	11.268	10.128	1.527
4338.7740	4338.7760	4338.7781	18.670	0.041	17.963	0.026	17.039	0.081	11.798	11.091	10.167	1.111
4339.8254	4339.8274	4339.8295	18.740	0.061	18.003	0.039	17.154	0.033	11.869	11.132	10.283	0.899
4342.5556	...	4342.5597	19.245	0.097	...	...	17.583	0.048	12.375	...	10.713	0.352
...	...	4342.8460	...	...	...	...	17.580	0.030	...	...	10.710	0.297
4343.5487	4343.5507	4343.5527	18.704	0.027	18.041	0.021	17.033	0.020	11.834	11.171	10.163	0.173
4343.8258	4343.8278	4343.8298	18.661	0.050	17.978	0.042	17.035	0.027	11.791	11.108	10.165	0.136
4344.7311	4344.7331	4344.7351	18.763	0.030	17.967	0.019	17.046	0.021	11.893	11.097	10.176	0.162
4344.8010	4344.8030	...	18.705	0.035	18.027	0.025	...	...	11.835	11.157	...	0.172
4345.6842	4345.6862	4345.6882	18.648	0.025	17.905	0.019	17.022	0.019	11.778	11.035	10.152	0.329
4345.7959	4345.7979	4345.7999	18.665	0.029	17.945	0.023	17.035	0.021	11.795	11.075	10.165	0.351
4346.5422	4346.5442	4346.5462	18.761	0.026	17.999	0.019	17.062	0.023	11.891	11.129	10.192	0.498
4346.8033	4346.8053	4346.8074	18.783	0.035	18.059	0.024	17.063	0.020	11.913	11.189	10.193	0.550
4347.7125	4347.7145	4347.7166	18.807	0.028	18.098	0.024	17.156	0.025	11.937	11.228	10.286	0.733
4347.8316	4347.8336	4347.8356	18.733	0.033	18.030	0.024	17.134	0.027	11.863	11.160	10.264	0.757
4348.7182	4348.7202	4348.7222	18.799	0.031	18.055	0.026	17.114	0.046	11.928	11.184	10.243	0.937
4348.7817	4348.7836	4348.7857	18.819	0.033	18.081	0.022	17.144	0.024	11.948	11.210	10.273	0.950
4349.6931	4349.6951	4349.6971	18.660	0.019	17.916	0.015	16.945	0.014	11.788	11.044	10.073	1.134
4349.7773	4349.7793	4349.7813	18.657	0.021	17.911	0.016	16.980	0.016	11.785	11.039	10.108	1.151
4350.6422	...	4350.6463	18.730	0.019	...	...	16.995	0.015	11.858	...	10.123	1.327
4350.8212	4350.6442	4350.8253	18.761	0.022	17.948	0.019	17.051	0.022	11.888	11.076	10.178	1.363
4351.7564	4350.8232	4351.7605	18.695	0.030	18.022	0.022	17.157	0.026	11.821	11.149	10.283	1.552
4352.7352	4351.7584	4352.7392	18.765	0.021	17.986	0.029	17.040	0.017	11.890	11.112	10.165	1.749
4353.7808	4352.7372	4353.7848	18.720	0.031	18.020	0.017	17.124	0.030	11.844	11.145	10.248	1.960
4354.8257	4353.7828	4354.8297	18.846	0.029	18.008	0.026	17.245	0.021	11.968	11.132	10.367	2.169
...	4355.7746	4355.7767	...	...	18.137	0.042	16.804	0.146	...	11.258	9.925	2.358
4356.7302	4356.7322	4356.7342	18.834	0.023	18.093	0.017	17.202	0.018	11.953	11.212	10.321	2.548
4357.7347	4357.7367	4357.7388	18.815	0.022	18.017	0.018	17.149	0.016	11.932	11.134	10.266	2.746
4358.7164	4358.7184	4358.7204	18.837	0.022	18.055	0.016	17.208	0.016	11.952	11.170	10.323	2.939
4360.7697	...	4360.7738	18.962	0.113	...	...	17.123	0.052	12.073	...	10.234	3.338
4362.6857	4362.6877	4362.6897	19.190	0.041	18.356	0.027	17.324	0.023	12.296	11.462	10.430	3.704
4364.6733	4364.6753	4364.6773	19.117	0.080	18.194	0.042	17.385	0.064	12.217	11.294	10.485	4.079
4365.6505	4365.6525	4365.6545	18.983	0.042	18.103	0.032	17.219	0.124	12.080	11.200	10.316	4.260
4370.7035	4370.7055	4370.7076	18.986	0.076	18.228	0.049	17.386	0.035	12.066	11.308	10.466	5.170
4371.6597	4371.6617	4371.6638	18.899	0.047	18.302	0.033	17.349	0.026	11.976	11.379	10.426	5.336
4372.6944	4372.6964	4372.6985	19.010	0.039	18.244	0.024	17.325	0.019	12.083	11.317	10.398	5.514

## (i) 51378 (2001 AT33)

JD (B)	JD (V)	JD (I)	B	$\sigma_B$	V	$\sigma_V$	I	$\sigma_I$	B <sub>red</sub>	V <sub>red</sub>	I <sub>red</sub>	Phase
4292.7792	4292.7811	4292.7831	19.846	0.052	19.137	0.038	18.145	0.035	13.029	12.320	11.328	2.839
4297.8408	4297.8430	4298.7235	19.641	0.087	18.779	0.158	18.119	0.034	12.834	11.972	11.313	1.809
4298.7195	4298.7215	...	19.897	0.043	19.108	0.033	...	...	13.091	12.302	...	1.628
4299.7540	4299.7560	4299.7580	19.933	0.039	19.127	0.035	18.124	0.035	13.128	12.322	11.319	1.414
4300.7167	4300.7186	4300.7207	19.989	0.038	19.175	0.030	18.210	0.031	13.185	12.371	11.406	1.215
4301.7707	4301.7726	4301.7746	19.888	0.038	19.131	0.031	18.152	0.034	13.086	12.329	11.350	0.997
4302.7282	4302.7302	4302.7322	19.866	0.047	19.170	0.035	18.157	0.032	13.064	12.368	11.355	0.800
4302.7902	4302.7922	4302.7942	19.803	0.044	19.156	0.034	18.217	0.032	13.002	12.355	11.416	0.787
4304.7293	4304.7313	4304.7333	19.975	0.053	19.164	0.039	18.190	0.040	13.175	12.364	11.390	0.396
4304.7588	4304.7607	4304.7628	19.920	0.072	19.023	0.052	18.169	0.054	13.120	12.223	11.369	0.390
4305.7043	4305.7063	4305.7083	19.799	0.095	18.894	0.068	17.986	0.051	12.999	12.094	11.186	0.220
4305.7432	4305.7452	4305.7472	19.700	0.133	19.040	0.096	18.001	0.074	12.900	12.240	11.201	0.214
4307.7136	4307.7156	4307.7176	19.917	0.076	19.104	0.044	18.129	0.034	13.118	12.305	11.330	0.300
4307.7513	4307.7533	4307.7554	19.924	0.068	19.149	0.043	18.144	0.035	13.125	12.350	11.345	0.307
4308.6467	4308.6486	4308.6507	19.845	0.089	18.905	0.047	18.120	0.043	13.046	12.106	11.321	0.480
...	4308.6900	4308.6921	...	...	19.489	0.106	18.238	0.062	...	12.690	11.439	0.488
4309.6919	4309.6939	4309.6959	19.950	0.146	19.032	0.088	18.134	0.087	13.150	12.232	11.334	0.691
4309.7429	4309.7448	4309.7468	20.022	0.139	19.031	0.135	18.191	0.071	13.222	12.231	11.391	0.702
4312.7454	4312.7473	4312.7493	20.162	0.206	18.990	0.087	18.448	0.107	13.361	12.189	11.647	1.321
4315.7138	4315.7158	4315.7178	19.853	0.097	19.058	0.052	18.061	0.059	13.049	12.254	11.257	1.934
4316.6944	4316.6964	4316.6984	19.753	0.050	19.004	0.035	18.091	0.031	12.948	12.199	11.286	2.135
4319.7203	4319.7222	...	19.791	0.040	19.040	0.030	...	...	12.981	12.230	...	2.751
4320.7184	4320.7204	4320.7224	19.774	0.041	19.009	0.029	18.025	0.029	12.962	12.197	11.213	2.952
4322.8091	4322.8111	4322.8131	19.814	0.073	19.124	0.058	18.189	0.071	12.998	12.308	11.373	3.369
4326.7450	4326.7470	4326.7490	19.816	0.051	19.100	0.036	18.128	0.037	12.990	12.274	11.302	4.137
4330.7181	4330.7200	4330.7221	19.774	0.043	19.020	0.034	18.046	0.034	12.936	12.182	11.208	4.884
4332.7624	4332.7644	4332.7664	19.831	0.064	19.051	0.046	18.117	0.045	12.986	12.206	11.272	5.256
4334.7178	4334.7198	4334.7218	19.681	0.058	19.077	0.044	18.096	0.038	12.829	12.225	11.244	5.604
4335.6537	4335.6557	4336.6241	19.752	0.085	18.991	0.057	18.024	0.056	12.897	12.135	11.165	5.767
4336.6200	4336.6220	4340.6927	19.649	0.143	18.963	0.095	18.044	0.059	12.790	12.104	11.167	5.933
4340.6887	4340.6907	4341.7024	19.687	0.135	18.973	0.084	18.209	0.053	12.810	12.096	11.328	6.608
4341.6984	4341.7004	4347.7067	19.675	0.126	19.145	0.117	18.293	0.097	12.794	12.264	11.383	6.769
4347.7027	4347.7047	4352.6665	19.957	0.101	19.106	0.082	18.230	0.038	13.047	12.196	11.293	7.668
4352.6625	4352.6645	4356.6813	19.942	0.047	19.173	0.035	18.272	0.046	13.005	12.236	11.313	8.332
4356.6773	4356.6793	4361.6563	19.935	0.054	19.159	0.044	17.875	0.040	12.976	12.200	10.886	8.815
4361.6523	4361.6543	4370.6416	19.980	0.087	19.043	0.050	18.655	0.092	12.991	12.054	11.610	9.341
4371.6016	4370.6395	4371.6057	20.331	0.152	19.688	0.139	18.710	0.065	13.280	12.643	11.659	10.091
4373.5823	4371.6036	4373.5864	20.465	0.063	19.693	0.096	18.828	0.055	13.401	12.642	11.764	10.155
4375.5706	4373.5843	4375.5747	20.386	0.138	19.710	0.045	18.881	0.098	13.309	12.646	11.804	10.280

**Table 3. Summary of Phase Curve Fits**

	$N_{\text{obs}}$	$\sigma_{\text{sys}}$	Linear Fit					Hapke Fit			
			S	$m_0$	$\chi^2$	$S_{\leq 2}$	$S_{> 5}$	$m_0$	$h_c$	$B_{c0}$	$\chi^2$
588 Achilles	38	0.02	0.04±0.01	8.41	36.5	0.05±0.02	0.04±0.02	8.40±0.01	10.3±0.5	1	44.9
1208 Troilus	12	0.02	0.05±0.02	9.08	10.1	0.06±0.03	...	9.08±0.01	7.4±0.5	1	10.5
4348 Poulydamas	9	0.08	0.09±0.04	9.75	7.1	0.04±0.09	...	9.74±0.03	4.7±1.0	1	11.8
6998 Tithonus	11	0.06	0.06±0.02	11.66	9.4	0.09±0.07	...	11.65±0.02	8.0±1.5	1	9.0
8317 Eurysaces	104	0.09	0.06±0.01	11.33	102.2	0.00±0.02	0.04±0.01	11.27±0.01	4.5±0.4	1	105.9
12126 (1999 RM11)	14	0.09	0.05±0.02	10.36	12.1	0.05±0.11	...	10.36±0.02	8.7±1.5	1	13.3
13323 (1998 SQ)	54	0.09	0.04±0.01	11.30	54.1	0.08±0.04	0.04±0.01	11.27±0.01	7.8±1.0	1	52.7
24506 (2001 BS15)	41	0.08	0.05±0.01	11.00	39.7	0.00±0.02	0.07±0.02	11.00±0.01	8.4±1.1	1	43.8
51378 (2001 AT33)	35	0.12	-0.02±0.01	12.23	33.1	-0.01±0.06	0.00±0.01	...	...	...	...

**Table 4. Comparison of Trojan Surface Properties with Other Bodies**

	$S_{\leq 2}$ (mag/°)	$N_{\leq 2}$	ref	$S_{>5}$ (mag/°)	$N_{>5}$	ref	B-R (mag)	ref	albedo (%)	ref
<b>Small/Gray Bodies</b>										
Trojans	0.00-0.09	8	1	0.04-0.07	5	1	1.0-1.5	4	3-6	8
Gray Centaurs	0.01-0.17	8	2	...			1.0-1.4	5	3-6	9
Gray SDOs	0.18	1	2	...			1.1-1.6	5	3-7	9
Dead Comet Candidates	...			...			1.0-1.5	6	2-9	8
<b>Transition Bodies</b>										
Active Centaurs	0.18	1	2	...			1.0-1.4	5	4-7	9
Active Comet Nuclei	...			...			0.9-1.6	7,12	2-6	7
<b>Small/Red Bodies</b>										
Red Centaurs	0.18	1	2	...			1.7-2.0	7	7-18	9
KBOs	0.10-0.25	13	2	...			1.5-2.0	7	6-16	9
<b>Main Belt Asteroids</b>										
D Class (non-Trojan)	...			...			1.4-1.5	11	4-6	11
P Class	0.075-0.113	4	3	0.039-0.044	4	3	1.2-1.5	11	2-7	11
C Class	0.065-0.127	9	3	0.039-0.046	9	3	1.2-1.6	10	3-9	11
M Class	0.145-0.197	6	3	0.029-0.036	6	3	1.3-1.5	10	7-30	11
S Class	0.151-0.196	9	3	0.024-0.032	9	3	1.5-2.0	10	4-50	11
E Class	0.084-0.138	4	3	0.018-0.022	4	3	1.1-1.5	10	16-55	11

References: (1) This work, not including 51378 (2001 AT33), which had an anomalous slope; (2) Schaefer et al. (2009a); (3) derived from individual fit parameters for each asteroid as reported in Belskaya and Shevchenko (2000); (4) Fornasier et al. (2007); (5) Tegler et al. (2003); (6) Jewitt (2002); (7) Lamy et al. (2004); (8) Fernandez et al. (2003); (9) Stansberry et al. (2008); (10) B-R values are calculated from the R/B values in Zellner (1979) using the formula  $B-R = 2.5 \log (R/B) + (B-R)_{\text{sun}}$ , with a value for  $(B-R)_{\text{sun}}$  of 1.19; (11) Compiled from the JPL Small-Body Database ([http://ssd.jpl.nasa.gov/sbdb\\_query.cgi#x](http://ssd.jpl.nasa.gov/sbdb_query.cgi#x)), with R/B values taken from Chapman and Gaffey (1979); B-R values were calculated as in (10); (12) Lamy and Toth (2009).

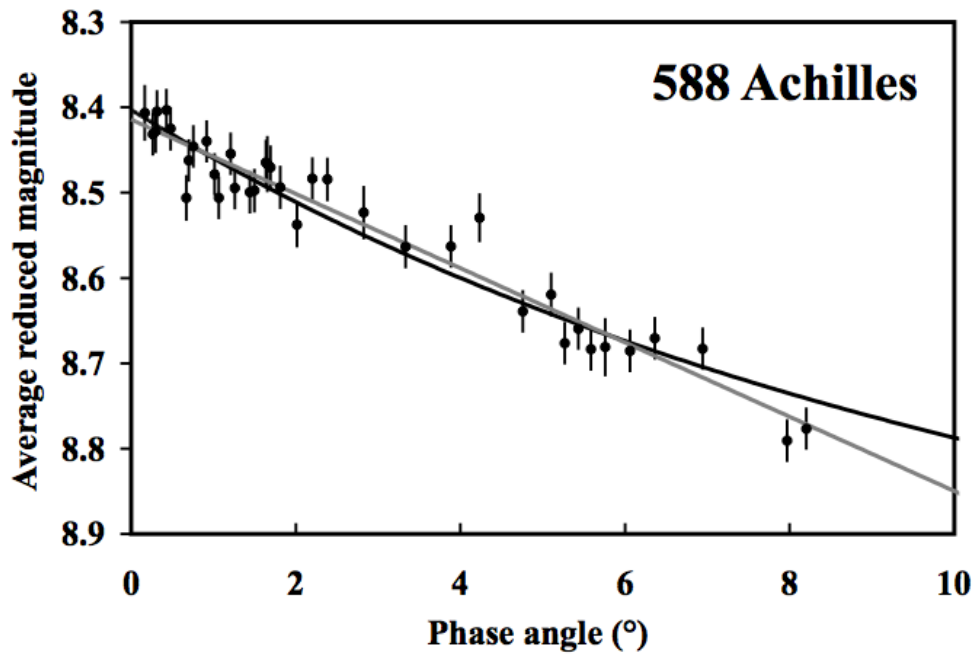


**Figure 1.** This phase curve for 588 Achilles is representative of all nine Trojan phase curves. It is a plot of the average reduced magnitude ( $m_{\text{avg}}$ ) versus the solar phase angle ( $\alpha$ ). The gray line represents the best linear fit, and the black line represents the best Hapke fit model. For Achilles, we have 38 magnitudes that consist of averages of our nearly-simultaneous B-, V-, and I-band magnitudes with corrections to a solar distance and geocentric distance of 1 AU. The one-sigma error bars plotted are the combined uncertainty from the measurement errors added in quadrature with an arbitrary systematic error ( $\sigma_{\text{sys}}$ , 0.02 mag in this case).

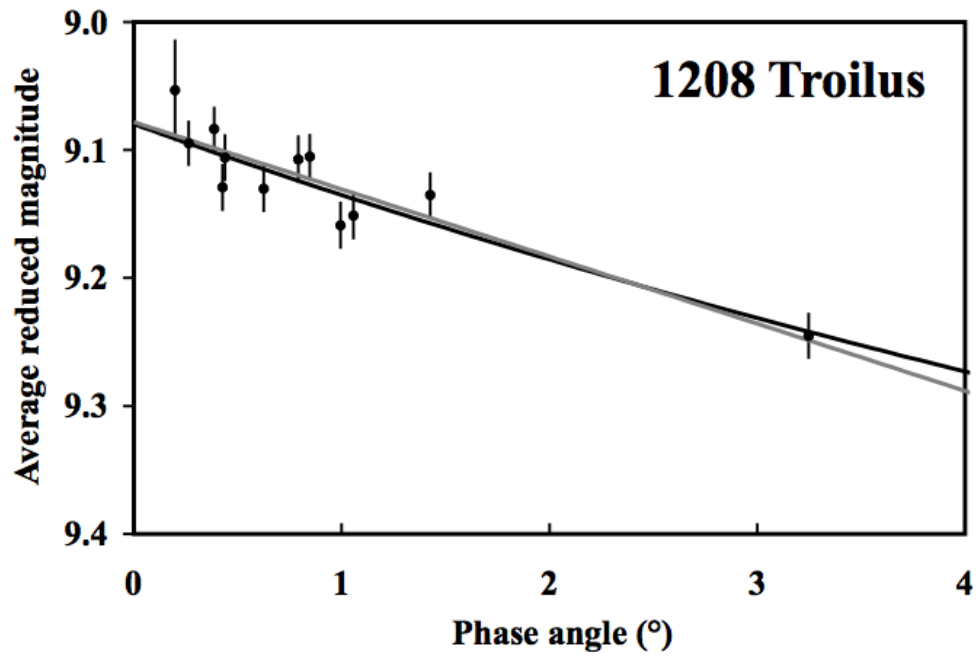


**Figure 2.** This phase curve for 1208 Troilus is the poorest-sampled in phase of our program. Nevertheless, the slope is well-measured, with a one-sigma uncertainty of  $\pm 0.02 \text{ mag}/^\circ$ . This slope is far larger than is possible by shadow-hiding alone, proving that coherent backscattering dominates in the opposition surge for this body.

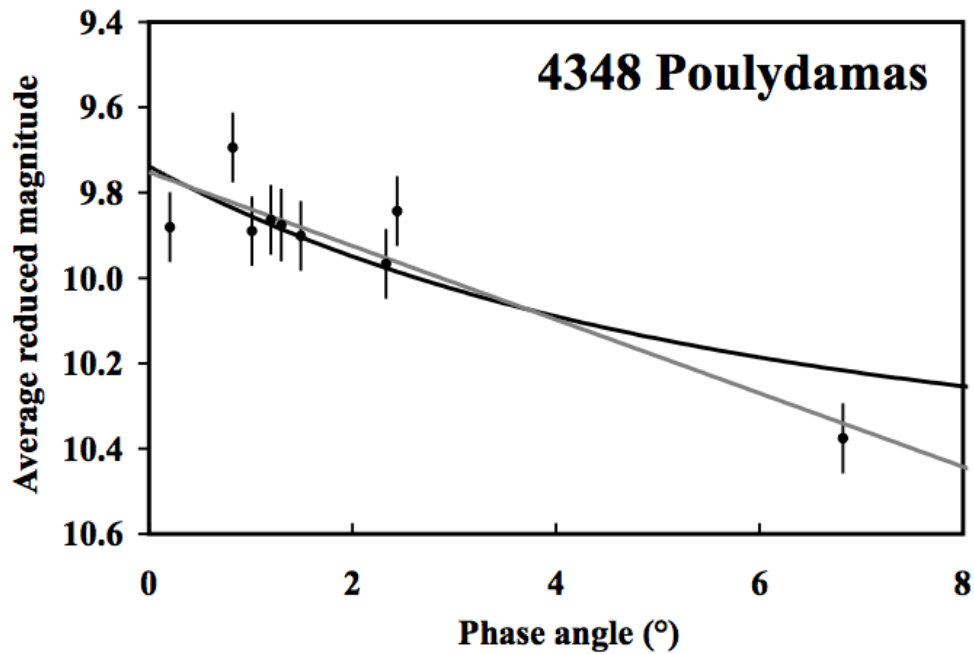


**Figure 3.** This phase curve for 4348 Poulydamas is easily consistent with a simple empirical linear fit. The linear model fits well ( $\chi^2=7.1$ ) and the Hapke model fits less well ( $\chi^2=11.8$ ). This difference in  $\chi^2$  shows that the linear fit is preferred at the 2-sigma confidence level. Almost all of this difference is caused by the one point at high phase angle where the Hapke model just can't get the value low enough due to the physical constraint that  $B_{C0} \leq 1$ .

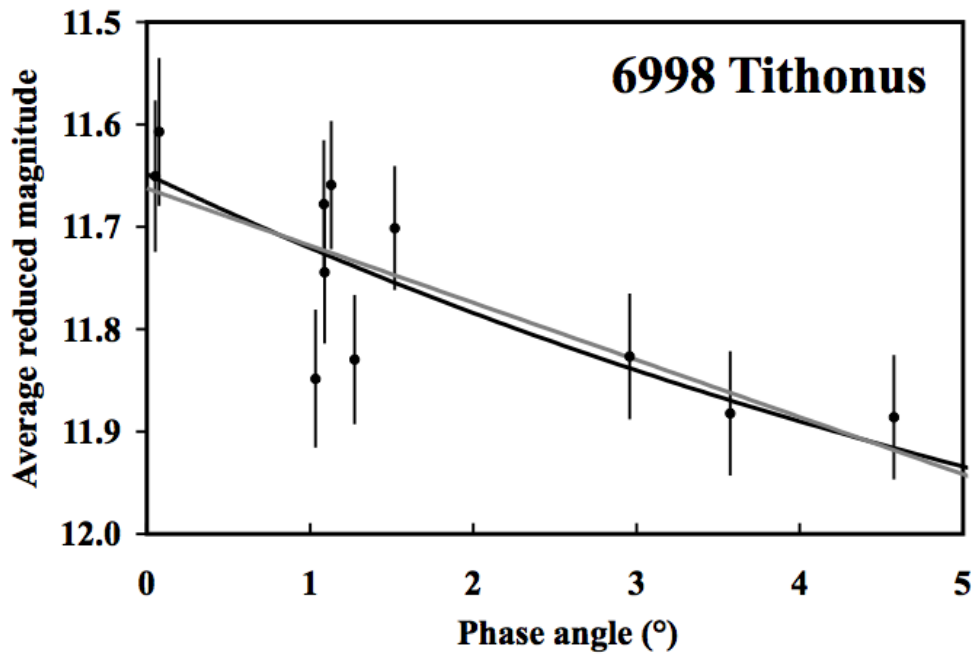


**Figure 4.** The phase curve of 6998 Tithonus appears to have a lot of scatter. With the given error bars, we see that nine out of eleven points are in agreement with either model to within one sigma. But this is illusory, because the quoted error bars have had an arbitrary uncertainty of  $\sigma_{\text{sys}}=0.06$  mag added in quadrature to the evaluated measurement errors. Therefore, apparently there is an extra variance in our data for Tithonus that has a typical scatter of 0.06 mag. We think that the most likely cause for this extra variance is uncorrected rotational modulation.

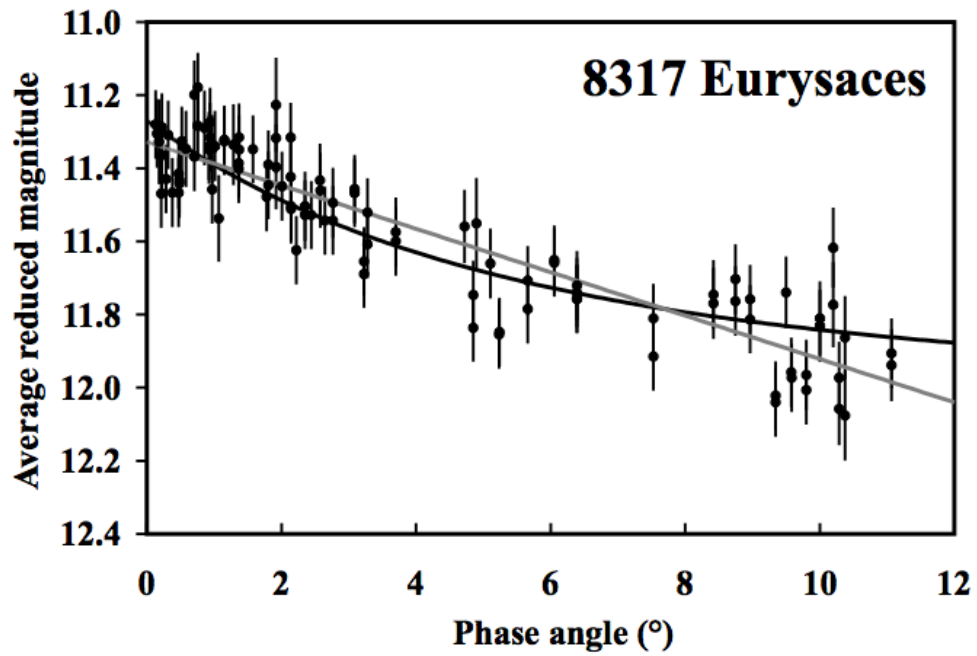


**Figure 5.** This phase curve for 8317 Eurysaces is constructed from two observing seasons (in 2006 and 2007) including 228 individual magnitude measurements (in B, V, and I) averaged together to for 104 points. This is our best-sampled phase curve. Even so, we could not pull out a rotational period with any confidence, primarily because our observing cadence was optimized for phase curves rather than rotational curves.

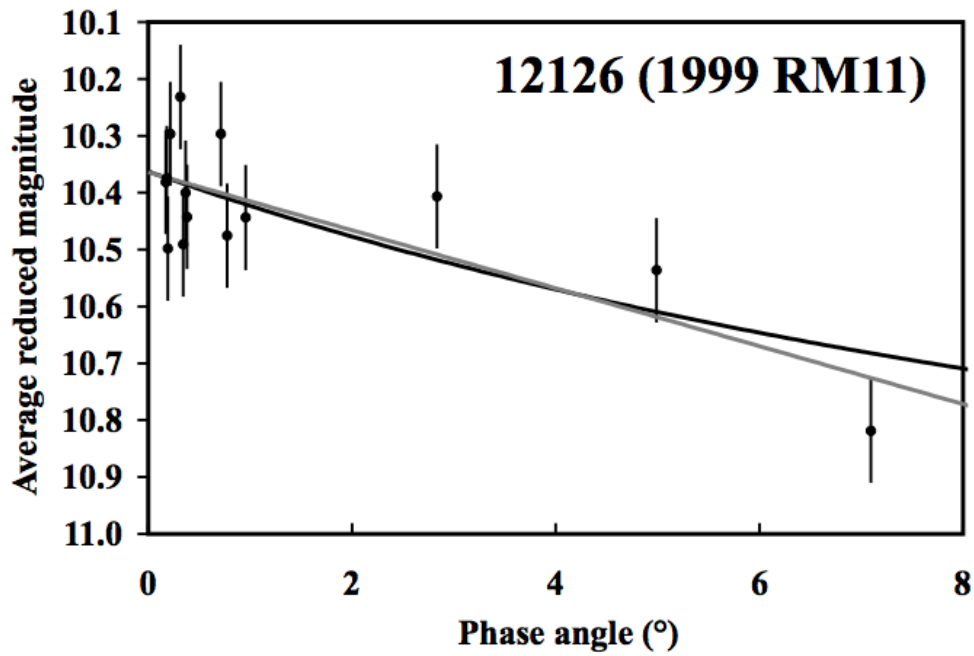


**Figure 6.** This phase curve of 12126 (1999 RM11) shows no significant difference between the linear and Hapke models. Indeed, all of our phase curves have no significant difference (at better than a 3-sigma confidence level) in  $\chi^2$  between the two models. This is to say that all our phase curves are adequately described by a simple straight line with no apparent curvature.

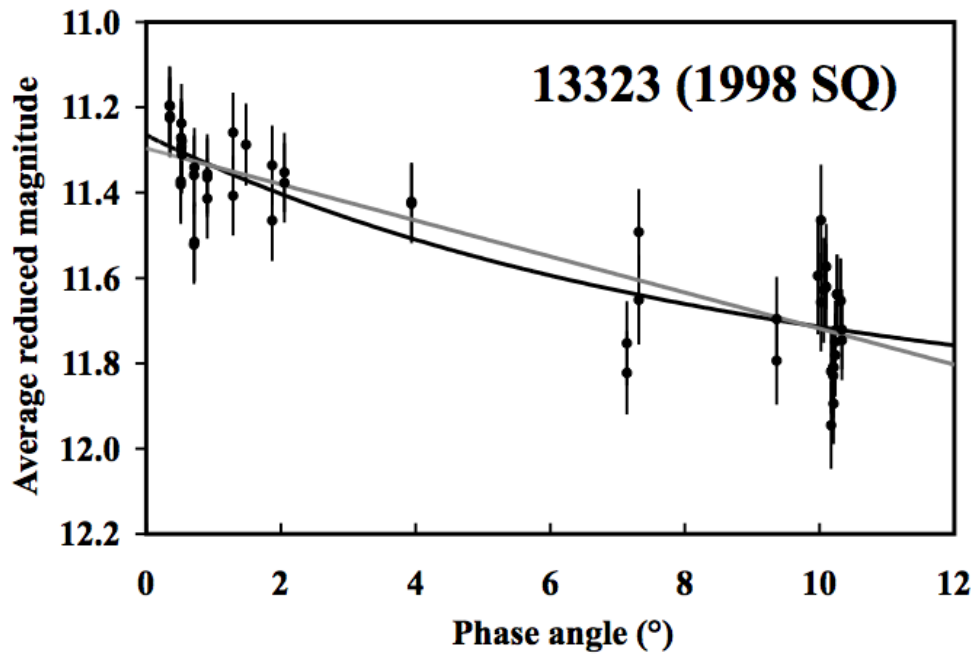


**Figure 7.** Again, in the phase curve for 13323 (1998 SQ) we see no significant difference here between the linear fit and the Hapke fit.

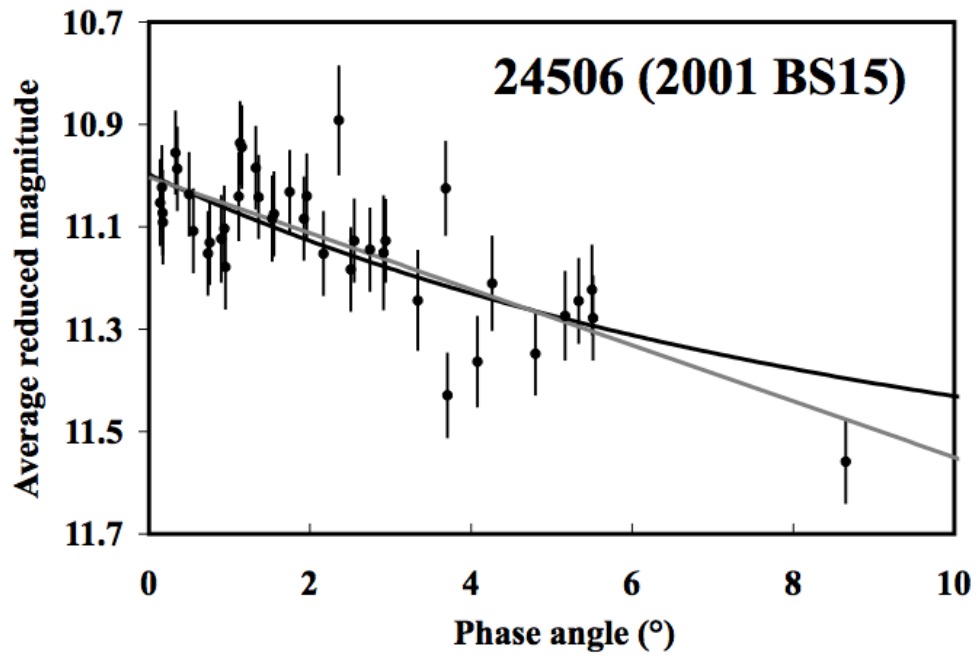


**Figure 8.** This phase curve for 24506 (2001 BS15) shows a small preference for the linear fit ( $\chi^2=39.7$ ) over the Hapke model ( $\chi^2=43.8$ ). Just as for 4348 Poulydamas (see Figure 3), the difference in  $\chi^2$  arises almost solely from the one high-phase point. Again, the reason why the Hapke model cannot better fit that point is the physical constraint that  $B_{C0} \leq 1$ .

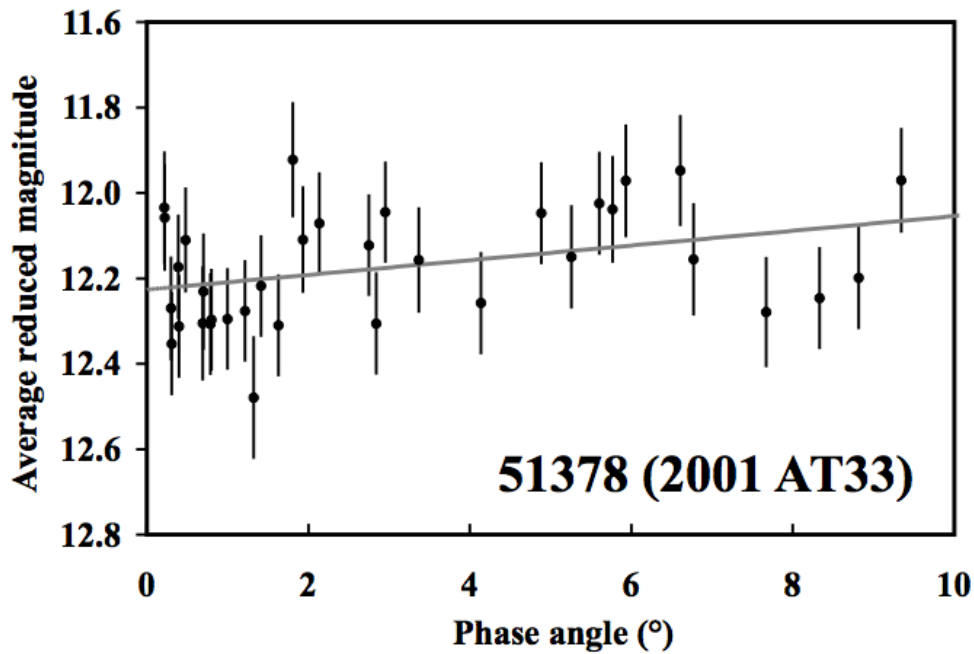


**Figure 9.** This phase curve for 51378 (2001 AT33) formally returns a negative slope from a linear fit. We know of no precedent or physical mechanism that can yield a negative slope. Likely, this Trojan simply has a near-zero opposition surge and ordinary variations (perhaps associated with rotational modulation) randomly result in a marginally negative slope. This idea is supported by the relatively large scatter of individual points (with  $\sigma_{\text{sys}}=0.12$  mag) that would arise for common rotational amplitudes if uncorrected.